Biochimica et Biophysica Acta 1858 (2016) 1635–1651

Contents lists available at ScienceDirect

Biochimica et Biophysica Acta

journal homepage: www.elsevier.com/locate/bbamem

Review

Molecular dynamics simulations of biological membranes and membrane proteins using enhanced conformational sampling algorithms☆

Takaharu Mori [a], Naoyuki Miyashita [b,c], Wonpil Im [d], Michael Feig [b,e,f], Yuji Sugita [a,b,f,g,*]

[a] iTHES Research Group and Theoretical Molecular Science Laboratory, RIKEN, 2-1 Hirosawa, Wako, Saitama 351-0198, Japan
[b] Laboratory for Biomolecular Function Simulation, RIKEN Quantitative Biology Center, Integrated Innovation Building 7F, 6-7-1 Minatojima-minamimachi, Chuo-ku, Kobe, Hyogo 650-0047, Japan
[c] Faculty of Biology-Oriented Science and Technology, KINDAI University, 930 Nishimitani, Kinokawa, Wakayama 649-6493, Japan
[d] Department of Molecular Sciences and Center for Computational Biology, The University of Kansas, 2030 Becker Drive, Lawrence, KS 66047, United States
[e] Department of Biochemistry and Molecular Biology, Michigan State University, East Lansing, MI 48824, United States
[f] Department of Chemistry, Michigan State University, East Lansing, MI 48824, United States
[g] Computational Biophysics Research Team, RIKEN Advanced Institute for Computational Science, 7-1-26 Minatojima-minamimachi, Chuo-ku, Kobe, Hyogo 650-0047, Japan

ARTICLE INFO

Article history:
Received 1 November 2015
Received in revised form 24 December 2015
Accepted 29 December 2015
Available online 5 January 2016

Keywords:
Generalized Born (GB) model
Generalized-ensemble algorithm
Replica-exchange molecular dynamics (REMD)
Replica-exchange umbrella sampling (REUS)
Surface-tension REMD
Replica exchange with solute tempering (REST)

ABSTRACT

This paper reviews various enhanced conformational sampling methods and explicit/implicit solvent/membrane models, as well as their recent applications to the exploration of the structure and dynamics of membranes and membrane proteins. Molecular dynamics simulations have become an essential tool to investigate biological problems, and their success relies on proper molecular models together with efficient conformational sampling methods. The implicit representation of solvent/membrane environments is reasonable approximation to the explicit all-atom models, considering the balance between computational cost and simulation accuracy. Implicit models can be easily combined with replica-exchange molecular dynamics methods to explore a wider conformational space of a protein. Other molecular models and enhanced conformational sampling methods are also briefly discussed. As application examples, we introduce recent simulation studies of glycophorin A, phospholamban, amyloid precursor protein, and mixed lipid bilayers and discuss the accuracy and efficiency of each simulation model and method. This article is part of a Special Issue entitled: Membrane Proteins edited by J.C. Gumbart and Sergei Noskov.

Contents

☆ This article is part of a Special Issue entitled: Membrane Proteins edited by J.C. Gumbart and Sergei Noskov.

* Corresponding author at: iTHES Research Group and Theoretical Molecular Science Laboratory, RIKEN, 2-1 Hirosawa, Wako, Saitama 351-0198, Japan.
E-mail address: sugita@riken.jp (Y. Sugita).

http://dx.doi.org/10.1016/j.bbamem.2015.12.032

1. Introduction

Biomembranes consist of various lipid molecules as well as membrane proteins [1]. Typical lipid molecules are amphiphilic and spontaneously form a bilayer where the hydrophobic acyl chains exist in the interior and the hydrophilic head groups facing outside [2]. Since ions, sugars, polypeptides, and other large substrates have difficulties in crossing the membrane hydrophobic core, membrane proteins such as channels, transporters, and pumps play key roles in facilitating their transport [3–6]. In order to communicate between cells as well as between a cell and its surrounding environments, membrane receptor proteins are responsible for signal transduction across membranes, mostly via conformational changes of the proteins [7–9]. These two biological phenomena, namely, substrate transports and signal transductions, are key functions of membrane proteins. Although atomic structural information of membrane transporters and receptors can greatly contribute to our understanding of such biological phenomena, their structure determination using X-ray, NMR, and cryo-EM techniques is still extremely challenging compared to soluble proteins. Consequently, the number of membrane protein structures in the Protein Data Bank (PDB: http://www.pdb.org) is much smaller than that of soluble proteins [10,11]. Moreover, many membrane proteins undergo large conformational changes during their functional cycles [12], implying that a single structure corresponding to just one of possible functional states of the protein is often not sufficient for understanding their biological function.

Theoretical and computational studies are expected to provide insight into these complex systems, which is difficult to obtain by experimental studies. Molecular dynamics (MD) simulation is a widely used computational tool to explore relationships between structure, dynamics, and function of biomolecules [13–16]. It has been applied to a wide variety of biomolecules, in particular proteins [17–19], nucleic acids [20–22], biomembranes [23–26], glycans [27–29], and so on. For biomembrane studies, most MD simulations before 2000 focused on simple phospholipid bilayers, such as DPPC (dipalmitoylphosphatidylcholine) or DMPC (dimyristoylphosphatidylcholine) bilayers [30–32]. Nowadays, MD simulations are applied to many membrane proteins in realistic cellular membrane environments [33,34] to examine conformational dynamics on the time scale of microseconds [35,36]. Furthermore, MD-special supercomputers, Anton [37] or Anton2 [38], make it possible to reach even longer time scales up to milliseconds so that biologically relevant events can be sampled frequently in a single MD trajectory [39–42]. In spite of these advances, many phenomena in biomembranes are still difficult to be simulated by conventional all-atom MD simulations because of limited simulation time scales. In particular, the transition time between the functional states of membrane proteins is generally much longer than what one can currently simulate. There are two possible approaches to potentially overcome these issues: the first involves simpler, but physically still realistic molecular models or representations for biomembrane systems; the other approach focuses on efficient conformational sampling algorithms. These two approaches can be combined to overcome the limitations of computational resources. In this review, we discuss both approaches in detail.

In biomembrane simulations, three main types of molecular models have been employed: all-atom [43–45], coarse-grained (CG) [46,47], and all-atom/CG mixed models [48–50]. Arguably, all-atom models are the most accurate, but it is computationally the most expensive. To extend the simulation time scales, different coarse-grained strategies have been developed to simplify the representation of proteins, water, and lipids [14]. One of the most popular models is the MARTINI model developed by Marrink and co-workers [47]. In this model, several atoms in proteins and lipids are approximated as a single united particle and four water molecules are treated as a single particle. Another popular model is the combination of an explicit protein representation with a mean-field solvent/membrane model such as the generalized Born (GB) model where the effects of solvent and membrane are included implicitly in the MD simulations [51,52]. Many MD simulations based on enhanced conformational sampling algorithms have been carried out with the GB models. Therefore, in this review, we discuss the GB models in detail because there are already many good review articles on MARTINI (and CG approaches) written by the original developers [53].

Enhanced conformational sampling methods for biomolecules have been actively developed by many theoretical and computational groups [54]. In this review, we mainly focus on the generalized-ensemble algorithm [55], which were originally developed in statistical physics [56]. Hansmann and Okamoto first applied the algorithm to the protein folding problem [57]. After that, various biological phenomena such as aggregation [58–60], large conformational changes of proteins [61], membrane protein folding and insertion [62–64], and protein–ligand binding [65,66] have been simulated using this algorithm. Here, we review replica-exchange MD (REMD) [67], replica-exchange umbrella sampling (REUS) [68], surface-tension REMD [69], and replica exchange with solute tempering (REST) [70] for biomembrane simulations. We also briefly discuss the accelerated MD (aMD) method [71].

To illustrate the accuracy and efficiency of different molecular models and enhanced sampling algorithms, we review recent simulations of glycophorin A (GpA) [72–75], phospholamban (PLN) [76–80], amyloid precursor protein (APP) [81–84], and mixed lipid bilayers [85–87]. In the simulations of GpA, PLN, and APP, REMD and REUS using implicit membrane models were mostly used to determine their conformational ensembles in membranes. Multi-scale molecular models including all-atom and CG models were also highly effective in the APP simulations. For mixed lipid bilayers, enhanced lateral diffusion and mixing were examined by REMD, surface-tension REMD, REST, and aMD with the all-atom model. This review concludes with perspectives in using MD simulations together with the enhanced conformational sampling algorithms in biomembrane studies.

2. Molecular models for membranes and membrane proteins

2.1. Implicit solvent and membrane models

2.1.1. Implicit solvent models

In most implicit solvent models based on continuum electrostatics, the solvent is approximated as a mean-field environment with a specific dielectric constant (ε) such as $\varepsilon = 80$ for water [88]. The resulting solvation free energy of a solute is then incorporated into the molecular mechanics potential energy function as an effective energy term [89]. Although detailed solute–solvent interactions are not considered, the solvation free energy can be reproduced reasonably with this approach. There are several advantages in using implicit solvent models. One advantage is increased computational efficiency because the computation of explicit solvent–solvent interactions, which is the most time-consuming part in explicit solvent MD simulations, is neglected. Therefore, implicit solvent simulations can easily reach microseconds with moderate computational resources [90,91]. This advantage is especially attractive in simulations of protein folding and large conformational changes that require longer time scales. Another advantage is a significant reduction in the degrees of freedom in a given system, which makes replica-exchange simulations effective using fewer replicas to achieve good overlaps in histograms between neighboring replicas (see below) [92]. The omission of the solvent degrees of freedom in an implicit model also means that solvent relaxation becomes instantaneous, which offers significant kinetic acceleration when modeling environments that reorganize slowly, such as membranes.

The solvation free energy is defined as the free energy change for transferring a given solute from vacuum to solution. When calculating solvation free energies, the following transfer process is often convenient: 1) removal of the partial charges and van der Waals interactions of a solute in vacuum, 2) creation of a solute cavity in solution, and 3) restoring the van der Waals interactions and partial charges of the solute inserted into the cavity within the solvent environment [93]. Therefore, the total solvation free energy, ΔG_{solv}, is usually decomposed as [94,95]:

$$\Delta G_{\mathrm{solv}} = \Delta G_{\mathrm{elec}} + \Delta G_{\mathrm{np}} = \Delta G_{\mathrm{elec}} + \Delta G_{\mathrm{cav}} + \Delta G_{\mathrm{vdW}}, \tag{1}$$

where ΔG_{elec} and ΔG_{np} are the electrostatic and nonpolar contributions to ΔG_{solv}, respectively. ΔG_{elec} includes direct interactions between solute partial charges and solvent as well as the screening of Coulombic interactions between solute charges. ΔG_{np} can be partitioned further into the free energy of cavity formation (ΔG_{cav}) and the free energy of solute–solvent van der Waals interactions (ΔG_{vdW}). In most implicit solvent models, ΔG_{np} is approximated as $\sum_i \sigma_i A_i$, where σ_i is an empirically derived coefficient and A_i is the solvent-accessible surface area (SASA) of the i-th atom. In the simplest approximation, a common value of σ is used for all atoms [95]. ΔG_{np} may also include an additional term representing solute–solvent van der Waals interactions separately [93,96].

2.1.2. Poisson–Boltzmann equation and generalized Born approaches

Based on the continuum electrostatic theory, ΔG_{elec} in Eq. (1) can be computed as $\Delta G_{\mathrm{elec}} = 1/2\sum_i q_i \phi_i(\mathbf{r}_i)$, where q_i is the partial charge and $\phi(\mathbf{r}_i)$ is the reaction field potential of the i-th solute atom. $\phi(\mathbf{r}_i)$ is obtained by solving the Poisson–Boltzmann (PB) equation:

$$\nabla \cdot [\varepsilon(\mathbf{r})\nabla\phi(\mathbf{r})] - \kappa^2(\mathbf{r})\phi(\mathbf{r}) = -4\pi\rho(\mathbf{r}), \tag{2}$$

where $\kappa(\mathbf{r})$ and $\rho(\mathbf{r})$ are the Debye–Hückel screening factor and the charge density of a solute, respectively. $\varepsilon(\mathbf{r})$ is the spatially-varying dielectric constant, which is typically set to a solute dielectric constant (ε_p) in the solute interior (usually 1) and a solvent dielectric constant (ε_w) for the solute exterior (80 for water). In the case that salt effects are not included, the PB equation reduces to the Poisson equation. The PB equation can be numerically solved by finite-difference methods [97–99]. The PB model is easily extended to heterogeneous environments like membrane systems by choosing an appropriate dielectric function [100], and it has been successfully applied for determining solvation free energy of biomolecules in membranes [101] as well as for including the transmembrane potential for solvation free energy calculations [102]. However, the direct solution of the PB equation is computationally expensive, and electrostatic forces cannot be simply described in terms of pairwise interactions between solute atoms. Therefore, the direct use of the PB equation in MD simulations is challenging [103].

An alternative approach for computing ΔG_{elec} is the generalized Born (GB) method, in which ΔG_{elec} is approximated as a sum of screened pairwise interactions between charges of a solute molecule: [94]

$$\Delta G_{\mathrm{elec}} = -\frac{1}{2}\left(\frac{1}{\varepsilon_{\mathrm{p}}} - \frac{1}{\varepsilon_{\mathrm{w}}}\right)\sum_{i,j}\frac{q_i q_j}{\sqrt{r_{ij}^2 + \alpha_i\alpha_j \exp\left(-r_{ij}^2/4\alpha_i\alpha_j\right)}}, \tag{3}$$

where q_i and q_j are the partial charges on the i-th and j-th atoms and r_{ij} is the distance between them. α_i is the effective Born radius of the i-th atom, which is typically estimated in the Coulomb field approximation, i.e.,

$$\frac{1}{\alpha_i} = \frac{1}{R_i} - \frac{1}{4\pi}\int_{\mathrm{solute}, r>R_i}\frac{1}{r^4}dV, \tag{4}$$

where R_i is the adjustable input radius of the i-th atom (mostly set to the atom's van der Waals radius), and the integral is carried out over the volume inside the solute but outside the i-th atom. If the effective Born radius is calculated accurately, the GB model can reproduce ΔG_{elec} obtained from the PB model [104,105]. Many efforts in developing practical applications of the GB model have focused on how to carry out the volume integral. Different approaches include a pairwise approximation [106–108], numerical surface/volume integration [94,109,110], additions of correction terms [111–113], introduction of rescaling parameters being proportional to the degree of the atom's burial [114], and the use of a smoothing function for the dielectric boundary [115], which yield different balances between accuracy and computational efficiency.

2.1.3. Extension to biological membrane systems

The GB model has also been extended to heterogeneous environments like membranes to simulate membrane proteins. In typical implicit membrane models, the dielectric constant of the protein interior is considered to be one, and the membrane region is treated as a low-dielectric slab (usually $\varepsilon = 1 - 4$) with a certain thickness embedded in a high-dielectric region to represent water and polar head-groups of membrane lipids [116,117]. In the first membrane GB model, called GBIM [118], the membrane is assumed to have the same dielectric constant as the proteins, so the system consists of two dielectric regions (Fig. 1a). The volume integral in Eq. (4) is split into two terms, where the integrals are taken over the solute space inside and outside the membrane individually. The integral over the membrane interior is approximated by an analytic function of a membrane thickness and the van der Waals radius and z-coordinate of a solute atom to reproduce ΔG_{elec} obtained from the PB model. The integral over the membrane exterior is computed by the pairwise method used for the implicit water model.

Im et al. proposed a different implicit membrane model, which is called the $\mathrm{GBSW_{MEMB}}$ model [119], an extension of GBSW in solution [115]. The $\mathrm{GBSW_{MEMB}}$ model assumes that the membrane has the same dielectric constant as the solute, and introduces a smoothing function at the dielectric boundary between the membrane hydrophobic core ($\varepsilon = 1$) and water ($\varepsilon = 80$) as well as between the solute ($\varepsilon = 1$) and water (Fig. 1b). This treatment makes the numerical calculation more stable at the membrane–water boundary. The model includes an

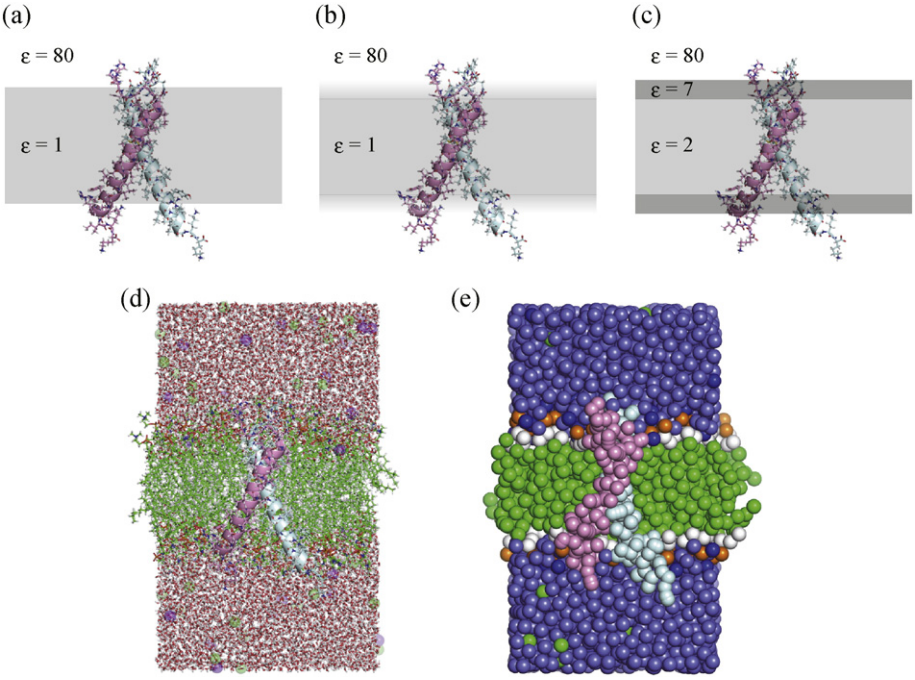

Fig. 1. Implicit and explicit membrane models. As an example, glycophorin A (GpA) is embedded in the membrane. (a) GBIM, (b) GBSW, (c) HDGB, (d) All-atom, and (e) MARTINI coarse-grained models.

empirical correction term to the Coulomb field term (Eq. (4)) [112], and the volume integral is carried out using quadrature techniques with radial and angular integration. The $GBSW_{MEMB}$ model reproduces the corresponding PB ΔG_{elec} within 2% absolute error with a confidence of about 95%.

Feig et al. proposed the HDGB model [120], where the dielectric constant varies along the membrane normal in order to model multiple layers with different dielectric constants (Fig. 1c). The membrane slab does not need to have the same dielectric constant as the solute. The varying dielectric constant is then used in Eq. (3) with Born radii α_i calculated as a function of the local value of ε. This model was optimized to reproduce the solvation free energy profile of a solute upon insertion into the explicit lipid bilayers [121]. The HDGB model has been further extended to allow dynamic membrane deformations with an additional energy term for the free energy of deformation from an elasticity theory [122].

2.1.4. Other implicit solvent and membrane models

Another implicit membrane model, different from the PB- or GB-based models, is the IMM1 model [123]. The IMM1 model is an extended form of the EEF1 model for soluble proteins [124]. Both EEF1 and IMM1 are computationally very efficient, even more than the GB models [125]. In the EEF1 model, the solvation free energy is given by

$$\Delta G_{solv} = \sum_i \Delta G_i^{ref} - \sum_i \sum_{i \neq j} f_i(r_{ij}) V_j, \tag{5}$$

where

$$f_i(r_{ij}) = \frac{\alpha_i}{4\pi r_{ij}^2} \exp\left\{ -\frac{(r_{ij} - R_i)^2}{\lambda_i^2} \right\}. \tag{6}$$

ΔG_i^{ref} is the reference solvation free energy of the i-th atom when it is fully exposed to solvent. V_i, R_i, λ_i, and α_i are the volume, van der Waals radius, correlation length, and proportionality coefficient of the i-th atom, respectively. The second term of Eq. (5) describes the effect of the surrounding atoms around the i-th atom. In the EEF1 model, ΔG_i^{ref} is derived from the experimental data of the solvation free energy for amino acid side-chain analogs in water. In the IMM1 model, ΔG_i^{ref} is re-defined by a combination of the solvation free energy of solute in water and cyclohexane:

$$\Delta G_i^{ref}(z') = f(z') \Delta G_i^{ref,water} + (1 - f(z')) \Delta G_i^{ref,cyclohexane}, \tag{7}$$

where $f(z')$ is a function describing the transition from one phase to the other:

$$f(z') = \frac{z'^n}{1 + z'^n}. \tag{8}$$

The exponent n controls the steepness of the transition, and $z' = |z|/(T/2)$, where T is the membrane thickness. Like EEF1, the IMM1 model uses a distance-dependent dielectric consent for the electrostatic calculation. However, the dielectric constant depends on the position of the interacting atoms with respect to the membrane. Far from the membrane, the dielectric constant is given by $\varepsilon = r$, which corresponds to the EEF1 model, while ε is close to one in the membrane center.

Recently, the IMM1 model has been extended to model lipid bilayers with a transmembrane potential [126,127], with aqueous pores [128,129], with anionic lipids [130], and mixed lipid bilayers with lateral pressure effects [131]. The transmembrane potential can be considered by introducing the analytical solution of the PB equation [102] or by introducing an empirical monotonic function along the membrane normal [126,127]. This method makes it possible to study mechanisms of voltage-dependent insertion of peptide and channel gating in the implicit solvent. In the IMM1 model with a cylindrical aqueous pore, an empirical function is introduced in Eq. (7) to describe the effects of the pore radius. MD simulations of β-barrel proteins with an implicit aqueous pore demonstrated that the proteins are more stable than in the standard IMM1 model [128]. To mimic the anionic lipid bilayers, the IMM1 model incorporates the Gouy–Chapman theory to describe the effect of a static surface charge on the membrane surface [130]. This model can deal with the electrostatic interactions between the lipid head groups and the solute, and it can be applied in the simulation of biologically active peptides, e.g. antimicrobial peptides. The membrane lateral pressure effects are considered by introducing the external

field describing the bilayer area expansion as well as pressure change caused by the compression of lipids upon solute insertion [131]. The model can describe mixed lipid-bilayers with a membrane lateral pressure profile that changes depending on the lipid composition [132].

2.1.5. Availability and applicability of the implicit solvent and membrane models

Implicit solvent and membrane models are available in many MD program packages such as CHARMM [133], AMBER [134], NAMD [135], GROMACS [136], TINKER [137], and IMPACT [138]. The PB model in AMBER can deal with both solvent and membrane systems, while the GB model is available for solvent. CHARMM supports all of the GB models as well as the EEF1/IMM1 model. The PB model in CHARMM is also available, but MD simulations are not practical. The *Implicit Solvent Modeler* available in CHARMM-GUI can facilitate the setup of implicit solvent simulations in CHARMM [139].

Recently, graphics processing units (GPUs) have become common for accelerating MD simulations with explicit solvent as well as implicit solvent [140,141]. The GB models in CHARMM/OpenMM, AMBER, NAMD, and GROMACS can utilize GPU and can produce hundreds of nanoseconds per day for small systems like Trp-cage and myoglobin [90,91]. A major bottleneck of GPU computation is the communication speed for copying data between CPU and GPU. To overcome this problem, MD simulation with the GB model in AMBER is performed mostly using the GPU, including force and energy evaluation and integration. The communication between the CPU and GPU takes place only when trajectory data need to be output [90]. In addition, computation with the GB model in mixed double and single precision on GPU has been demonstrated to be fast and can reproduce the results in double precision on CPU [90]. An efficient GB/SA calculation scheme was also introduced into NAMD, in which the GB term is computed on the GPU while the SA term is calculated on the CPU, thereby implementing a hybrid CPU/GPU architecture [142].

In general, the GB model is the most useful for simulating relatively small protein molecules, where the computational time for the GB term is usually only a few times slower than that for gas-phase simulations and where fully solvated systems would contain much more solvent atoms than solute atoms. Since the GB models use a cut-off scheme for the calculation of non-bonded interactions, the cut-off distance should be large enough (usually 16–20 Å or more for membrane systems) to maintain an accurate calculation of long-range electrostatic interactions. This creates additional computational costs compared to explicit solvent simulations where 10–12 Å are the typical cut-off distance for van der Waals interactions and the real space for the particle mesh Ewald (PME) method [143] for electrostatic interactions. Furthermore, the PME method can be efficiently parallelized via domain decomposition schemes for accurate and fast electrostatic calculations [144]. As a result, the calculation of the GB energy and forces can be more expensive than those in the explicit solvent model for large systems like the ribosome. To overcome this problem, a hierarchical charge partitioning (HCP) scheme has been proposed to achieve $N\log N$ scaling, where the atoms far from focusing given central atom are approximated to one particle with a point charge and a corresponding effective Born radius [145]. The HCP method can offer significant speed-up over the conventional GB method in particular for large systems. In NAMD, the GB computation is parallelized by the combination of domain decomposition and force decomposition schemes to realize balanced workload between high- and low-density domains [146].

2.2. Explicit solvent and membrane models

2.2.1. All-atom models for membranes and membrane proteins

In contrast to implicit solvent models, explicit solvent models include fully detailed interactions between a solute and solvent, and between solvent and solvent. In MD simulations with explicit solvent and membranes, the all-atom model is widely used, where one atom is described by one particle with an atomic mass, a partial charge, and a van der Waals radius (Fig. 1d). The all-atom model can be further extended to include polarizability, such as the Drude model, where a massless and charged particle is attached to a polarizable atom via a harmonic spring [147,148].

There are mainly two important considerations in performing MD simulations with all-atom membrane models. First, the choice of force field parameters and nonbonded cut-off options is critical for the success of simulations [149]. In MD simulations with previous CHARMM27 [150] or AMBER Lipid11 force fields [151], lipid tail groups showed a bias toward all-trans conformations, which yielded reduced area per lipid values in MD simulation in the *NPT* (constant particle number, pressure, and temperature) ensemble compared to the experiments [152]. To overcome this problem, *NPAT* (constant particle number, normal pressure, area, and temperature) and *NPγT* (constant particle number, normal pressure, surface tension, and temperature) ensembles had to be used, so that the area per lipid was maintained close to the target experimental value [153]. The recently optimized lipid force-field parameters (CHARMM36 [43] and AMBER Lipid14 [45]) show excellent agreement with experimental structural properties of lipid bilayers such as the area per lipid, membrane thickness, and order parameters in the *NPT* ensemble.

Second, careful modeling of a protein–membrane complex is necessary. The initial orientation of a protein with respect to the bilayer plane should be reasonably determined before starting MD simulations. For this, the OPM database (http://opm.phar.umich.edu) can be used, which provides PDB coordinates of membrane proteins in the optimal orientation predicted by minimizing the solvation free energy in membranes [154]. After determining the orientation, a membrane protein is embedded into an explicit lipid bilayer. Many protocols have been proposed to construct a reasonable initial structure of a protein–membrane complex [155–159]. CHARMM-GUI *Membrane Builder* is widely used for system building in homogenous or mixed bilayers with more than 180 lipid types available [160,161]. It also provides well-validated equilibration and production inputs for many MD program packages (CHARMM, NAMD, GROMACS, AMBER, OpenMM, and CHARMM/OpenMM) [162]. While it is difficult to estimate the correct number of lipids in each leaflet of protein–membrane systems to avoid a mismatch in lipid packing, it has been suggested that the area per lipid mismatch up to 5% would be tolerable in membrane simulations of typical all-atom system sizes [163]. For the analysis of the area per lipid in protein–membrane systems, the Voronoi tessellation Monte Carlo integration method has been proposed [164], which also makes possible to assess equilibration of lipid bilayers by comparing the obtained area per lipid with the experimental data.

2.2.2. Coarse-grained and all-atom/coarse-grained mixed models

An alternative to all-atom membrane and protein–membrane models are coarse-grained (CG) models. In CG models, several atoms are combined into one particle with a certain mass, radius, and charge (Fig. 1e). Several CG models have been developed previously [165], among which MARTINI is the most popular and widely used model for lipids as well as proteins [47]. In MARTINI, four heavy atoms and their associated hydrogen atoms are grouped together into a single particle (four-to-one mapping). MARTINI has been applied to investigate large-scale and long-time scale biological phenomena such as membrane domain formation [166], crowding [167], peptide insertion [168], and channel gating [169]. However, the model requires knowledge-based secondary structure restraints to simulate proteins in the membrane. To overcome this problem, the backbone pseudo-dihedral potential has been recently introduced to the MARTINI model in order to reproduce internal dynamics of proteins [170].

Multi-scale or mixed resolution models have also been developed [48,171]. Feig et al. proposed the PRIMO model, in which the CG interaction sites are chosen so that an analytic reconstruction from the CG to all-atom model is possible [172,173]. In addition, the model can

combine CG and all-atom particles at the same time during MD simulations. Recently, PRIMO was extended to PRIMO-M that can be used with the GB model to simulate membrane-inserted peptides [50]. Wu et al. developed the PACE force field, which is used to simulate protein–membrane systems with the united-atom model for proteins and the MARTINI model for water and lipids [49,174]. They demonstrated that the orientation of WALP peptides and the predicted structure of the GpA dimer are well in agreement with the experimental data. Recently, the *PACE CG Builder* and *Martini Maker* have been developed and added to CHARMM-GUI, to allow the automatic setup of various systems with PACE and MARTINI force fields [175,176].

3. Enhanced conformational sampling methods

3.1. Replica-exchange molecular dynamics (REMD) method

3.1.1. Temperature REMD

The replica-exchange molecular dynamics (REMD) method is one of the enhanced conformational sampling methods used for systems with rugged free-energy landscapes. The original temperature-exchange method (T-REMD) is used most widely in biomolecular simulations [67]. In T-REMD, replicas (or copies) of the original system are prepared, and different temperatures are assigned to each replica. Each replica is run in an *NVT* [67] or *NPT* ensemble [177], and target temperatures are exchanged between a pair of replicas during the simulation (Fig. 2a). Exchanging temperature enforces a random walk in temperature space, resulting in the simulation surmounting energy barriers and the sampling of a much wider conformational space of target molecules. The transition probability from state X to X' in the replica-exchange process is given by the Metropolis criterion:

$$w(X\to X') = \begin{cases} 1, & \text{for } \Delta\le 0, \\ \exp(-\Delta), & \text{for } \Delta>0, \end{cases} \tag{9}$$

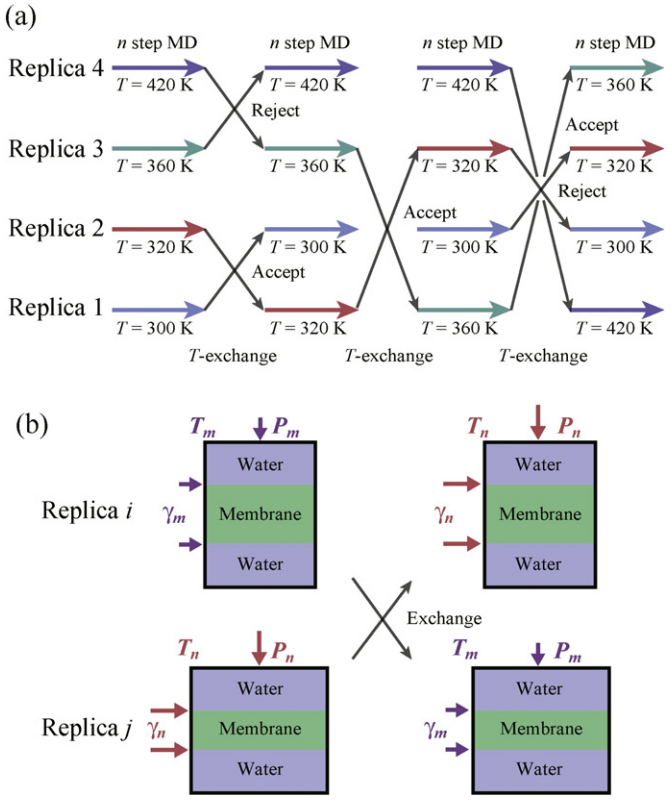

Fig. 2. Replica-exchange schemes in (a) T-REMD and (b) surface-tension REMD.

with

$$\Delta = (\beta_m-\beta_n)\left\{E\left(q^{[j]}\right)-E\left(q^{[i]}\right)\right\}, \tag{10}$$

where E is the potential energy, q is the position of atoms, β is the inverse temperature defined by $\beta = 1/k_BT$, i and j are the replica indexes, and m and n are the temperature indexes. After the replica exchange, atomic momenta are rescaled as follows:

$$p^{[i]'} = \sqrt{\frac{T_n}{T_m}}p^{[i]}, \qquad p^{[j]'} = \sqrt{\frac{T_m}{T_n}}p^{[j]} \tag{11}$$

where p are the momenta of atoms. The transition probability should be independent of constant temperature and constant pressure algorithms, whereas the momenta-rescaling scheme depends on the algorithm used in the simulation. If thermostat and barostat momenta are included in the equations of motion like the Martyna–Tobias–Klein algorithm [178], these variables should also be rescaled after replica exchange [179,180]. The results from T-REMD simulation can be analyzed by reweighting techniques such as the weighted histogram analysis method (WHAM) [181,182].

3.1.2. Replica-exchange umbrella sampling (REUS)

The umbrella sampling (US) method has been widely used to calculate free energy profiles of physical and/or chemical processes along reaction coordinates [183]. In this method, an umbrella potential (or biasing potential) is imposed to sample conformations around a target value along a reaction coordinate, and a series of independent simulations with different umbrella potentials are performed to cover the entire range of a given reaction coordinate. If a sufficient overlap between histograms of neighboring umbrellas is obtained, reweighting techniques such as WHAM can be used to combine individual simulations and calculate the free energy profile [184]. To perform US simulation, the choice of the umbrella potential parameters is important. If the force constant of the umbrella potential is too strong, each simulation samples a very narrow conformational space, requiring too many simulations for covering the entire reaction coordinate. Efficient sampling methods based on the idea of US have been developed, such as λ-dynamics [185].

Sugita and Okamoto proposed the replica-exchange umbrella sampling method (REUS [68], this method is also referred to as Hamiltonian REMD [186] or window-exchange USMD [187]), where each simulation is run with different umbrella potentials and they are exchanged between a pair of replicas (or windows) during the simulation. The potential energy of the system in the replica i is given by the summation of the original potential energy E_0 and the umbrella potential V with the coupling parameter λ_m,

$$E_{\lambda_m}\left(q^{[i]}\right) = E_0\left(q^{[i]}\right) + V_m\left(q^{[i]}\right), \tag{12}$$

where V_m depends on the parameter λ_m, which can also be written as $\lambda_m V(q^{[i]})$. The transition probability for a replica exchange scheme is given by the Metropolis criterion as in Eq. (10) and

$$\Delta = \beta\left(V_m\left(q^{[j]}\right)-V_m\left(q^{[i]}\right)-V_n\left(q^{[j]}\right)+V_n\left(q^{[i]}\right)\right). \tag{13}$$

The computational cost of REUS is the same as for US, when the number of replicas (or umbrella potentials) is the same. However, all the replicas have to be simulated simultaneously on a massively parallel computing architecture, requiring very large computer resources, when REUS simulations for large biological systems are carried out. Nonetheless, the advantage of REUS over US is that the continuity of states along the reaction coordinate is guaranteed, because umbrella potentials are exchanged between neighboring λ conditions. To further improve sampling efficiency, REUS has also been combined with other enhanced

sampling methods such as REMD [68] and replica-exchange solute tempering (REST/REUS; for REST, see the section below) [66]. Recently, Park et al. derived an analytical expression for the average acceptance probability between neighboring replicas (or windows) and combined it with the first passage time optimization method to predetermine a pair of optimal US parameters, k (the window force constant) and d (the window spacing): $k^{1/2}d = 0.8643(2k_BT)^{1/2}$ [187].

3.1.3. Surface-tension REMD

Surface tension is a force arising at liquid interfaces such as in vacuum/water, oil/water, and membrane/water systems. In the case of a lipid bilayer/water system, the surface tension is zero when the bilayer is ideally flat [188]. Positive surface tension increases the surface area of a lipid bilayer, while the thickness decreases due to volume incompressibility [2]. The surface-tension REMD (γ-REMD) method is an enhanced conformational sampling method that is specialized for biological membrane systems [69]. In this method, each replica is simulated in the *NPγT* ensemble [153], and target surface tension values are exchanged between a pair of replicas. Accordingly, the γ-REMD method aims at enhancing structural changes of molecules in membranes mechanically.

If one considers an orthorhombic simulation box with lengths of h_x, h_y, and h_z and a lipid bilayer parallel to the xy plane, the surface tension of the system is defined as

$$\gamma = h_z \times \left(P_{zz} - \frac{P_{xx} + P_{yy}}{2} \right), \tag{14}$$

where P_{zz} is the normal pressure, and P_{xx} and P_{yy} are the tangential components of the pressure tensor. The replica exchange scheme in the γ-REMD method is basically the same as in T-REMD. The transition probability for the replica-exchange process (Fig. 2b) is given by the Metropolis criterion as in Eq. (10):

$$\begin{aligned} \Delta = {} & (\beta_m - \beta_n)\left\{ E\left(q^{[j]}, h^{[j]}\right) - E(q^{[i]}, h^{[i]}) \right\} \\ & + (\beta_m P_m - \beta_n P_n)\left(h_x^{[j]} h_y^{[j]} h_z^{[j]} - h_x^{[i]} h_y^{[i]} h_z^{[i]} \right) \\ & - (\beta_m \gamma_m - \beta_n \gamma_n)\left(h_x^{[j]} h_y^{[j]} - h_x^{[i]} h_y^{[i]} \right), \end{aligned} \tag{15}$$

where P is the normal pressure. Based on this equation, surface tension can be exchanged multi-dimensionally with temperature (γT-REMD), normal pressure (γP-REMD), or both of them (γPT-REMD).

Mori et al. applied the γ-REMD method to a pure DPPC lipid bilayer, and they found that lateral diffusion of lipid molecules is enhanced compared to a standard *NPT* MD simulation [69]. This can be understood in terms of free-area effects [189] in the expanded structures of the membrane. They also carried out γ-REMD simulations of the WALP23 peptide in POPC lipid bilayers, and calculated the free energy profile as a function of tilt angle of WALP23. The γ-REMD method induced reorientation of WALP23 due to protein–lipid interactions, resulting in more accurate free energy profile than in *NPT* MD simulations. They further performed γT-REMD, γ-REMD, and T-REMD simulations of mixed POPC/DMPC lipids, whose results are described below in detail in terms of the effect of surface tension on membrane structures [87].

3.2. Other enhanced sampling methods

3.2.1. Replica exchange with solute tempering (REST)

Although REMD is applicable to many systems, the number of replicas required for efficient sampling scales as $\sqrt{f}$ (where f is the number of degrees of freedom), implying that a large number of replicas are necessary for simulating large systems. To overcome this problem, the replica exchange with solute tempering (REST) method has been proposed, in which only the solute molecule is heated up, while the solvent stays cold even in high temperature replicas [70]. REST is one of Hamiltonian REMD methods, where solute tempering is achieved by scaling solute–solvent and solvent–solvent interactions (REST1) [70] or solute–solvent and solute–solute interactions (REST2) [190,191].

In REST1, the potential energy of the system for replica m is given by

$$E_m(q) = E_{pp}(q) + \frac{\beta_0 + \beta_m}{2\beta_m} E_{pw}(q) + \frac{\beta_m}{\beta_0} E_{ww}(q), \tag{16}$$

where E_{pp}, E_{pw}, and E_{ww} are protein–protein, protein–water, water–water interactions, respectively. With $\beta_0 = 1/k_BT_0$ for the target temperature T_0, the acceptance criterion for the replica exchange is determined similarly as in other replica-exchange methods:

$$\Delta = (\beta_m - \beta_n)\left[(E_{pp}(q_n) - E_{pp}(q_m)) + \frac{1}{2}(E_{pw}(q_n) - E_{pw}(q_m)) \right]. \tag{17}$$

In Eq. (17), the water–water interactions terms are canceled out, which allows us to use smaller number of replicas required for efficient conformational sampling. In REST1 simulations, each replica is run at different temperature and has different potential energy function. REST1 simulation was shown to be more efficient than T-REMD for a small solute system like the alanine dipeptide [70]. In contrast, simulations for a large system involving large conformational changes were less efficient than T-REMD.

To overcome this problem, REST2 has been developed [190,191], in which the potential energy of the system for replica m is given by

$$E_m(q) = \frac{\beta_m}{\beta_0} E_{pp}(q) + \sqrt{\frac{\beta_m}{\beta_0}} E_{pw}(q) + E_{ww}(q), \tag{18}$$

and the acceptance criterion for the replica exchange becomes

$$\begin{aligned} \Delta = {} & (\beta_m - \beta_n) \\ & \times \left[(E_{pp}(q_n) - E_{pp}(q_m)) + \frac{\sqrt{\beta_0}}{\sqrt{\beta_m} + \sqrt{\beta_n}} (E_{pw}(q_n) - E_{pw}(q_m)) \right]. \end{aligned} \tag{19}$$

In REST2 simulations, all the replicas are run at the same temperature T_0, while each replica has a different scaling factor for the potential energy. A comparison between T-REMD, REST1, and REST2 on folding simulations of Trp-cage and β-hairpin indicated that REST2 is the most efficient one for larger systems [191].

Another method based on the idea of solute tempering has also been proposed by Moors et al. [192]. They introduced the replica exchange with flexible tempering method, in which a part of the solute molecule, e.g., flexible hinges or loops of the protein, is heated up in order to enhance domain motions of proteins.

3.2.2. Accelerated molecular dynamics (aMD)

In the accelerated MD (aMD) method [71], conformational transitions between different states are enhanced by adding a bias potential to the potential energy:

$$E^*(q) = E(q) + \Delta E(q), \tag{20}$$

where $E(q)$ is the original potential energy, and $\Delta E(q)$ is called the boost potential defined by

$$\Delta E(q) = \begin{cases} 0, & \text{for } E(q) \geq E_{\text{cut}}, \\ \dfrac{(E_{\text{cut}} - E(q))^2}{\alpha + E_{\text{cut}} - E(q)}, & \text{for } E(q) < E_{\text{cut}}, \end{cases} \tag{21}$$

where E_{cut} is the energy threshold that determines whether the system is biased or unbiased. When the potential energy is greater than E_{cut}, the simulation is run on the original potential energy surface $E(q)$. The acceleration factor α determines the depth of the modified potential energy surface. The choice of E_{cut} and α is very important, and may require a trial-and-error search for each system. As α increases, the modified potential energy surface becomes close to the original one. As α

decreases, the modified energy surface becomes more flat. When E_{cut} is very high and α is very small, the modified potential becomes isoenergetic in most place of the energy landscape, and the simulation shows a random walk. One way to choose E_{cut} is to use an average of the original potential energy distribution obtained from a short unbiased MD simulation for the target system.

Recently, Miao et al. proposed the Gaussian accelerated MD method (GaMD), where a harmonic boost potential is used instead of Eq. (21) to smoothen the potential energy surface [193]. They suggested that this treatment could reduce energetic noise during reweighting and yield an accurate free energy profile.

4. Recent membrane and membrane protein simulations using enhanced conformational sampling methods

4.1. Glycophorin A (GpA)

Glycophorin A (GpA) is an antigen-presenting protein on the surface of human erythrocytes. Its transmembrane (TM) dimer structure was determined by solution nuclear magnetic resonance (NMR) spectroscopy in detergent micelles (PDB ID: 1AFO) [194] and in lipid bicelles (PDB ID: 2KPE, 2KPF) [195]. GpA has long been a model protein to investigate structure and stability of membrane protein dimers in different membrane environments [196,197] as well as a popular target of membrane simulations [72,74,75,119,123,187,198]. The transmembrane sequence of GpA contains the "GxxxG" motif (Table 1), which is often observed at TM–TM contact interfaces of membrane proteins [199,200]. This motif as well as its variants "G(A)xxxG(A)" can form an interhelical backbone hydrogen bond that enhances dimer stability in membranes. In addition, β-branched residues (Val, Leu, and Ile) adjacent to the "GxxxG" motif contribute to the enhanced stability of GpA dimer structure.

Since it is not feasible to predict TM helix dimers using conventional all-atom MD simulations, the MD simulation studies for the GpA dimer prediction have combined various implicit membrane models and several enhanced conformational sampling methods such as US [72,75], replica-exchange Monte Carlo (REMC) [198], T-REMD [75,77,119], and REUS [74]. Toward reliable modeling/simulation of the TM helix dimer, it is necessary to examine accuracy and efficiency of molecular models and simulation methods. Here, we discuss the choices of (i) reaction coordinates in US and REUS, (ii) sampling algorithms (US vs T-REMD), and (iii) implicit membrane models (IMM1 vs $GBSW_{MEMB}$) in the simulations.

In general, the structure of a TM helix homodimer is described by three internal coordinates, namely, interhelical distance (R), interhelical crossing angle (Ω), and relative rotational angle (ρ), if we assume each TM helix as a rigid rod and the TM helix homodimer is symmetric (Fig. 3a). Henin et al. performed US simulations of a GpA dimer using only the interhelical distance R as a reaction coordinate in an all-atom POPC bilayer [72]. They defined the interhelical distance as the distance separating the centers of mass (COM) of the two TM helices. In their simulations, the potential of mean force (PMF) for the reversible dimerization of the GpA dimer was estimated, and a mechanism was suggested where the early recognition stage was primarily driven by van der Waals TM helix interactions. Although this simulation agreed with the "two-stage" model of integral membrane protein folding [201], the sampling efficiency of other degrees of freedom was not clear. Lee et al. developed the restraint potentials by which the distance and crossing angle of two helices are kept around target values in MD simulations [202]. In this potential, the interhelical distance is defined as the minimum distance between two TM helices. This was applied in the study of generic TM dimer formation in an all-atom DMPC bilayer [203]. In addition, using such a helix restraint potential, Park et al. compared the conformational sampling efficiency for the one-dimensional (1d) REUS with R as the reaction coordinate to the two-dimensional (2d) REUS with R and Ω as the reaction coordinates [74]. They demonstrated that the high barrier along Ω in the free-energy landscape prevents efficient sampling along R, and thus the 2d-REUS is a general and efficient approach to studying TM helix dimerization.

Recently, Li et al. defined three points in each helix A and B (X1, X2, X3, where X = A or B) for describing three internal coordinates, R, Ω, and ρ [75]. X1 and X2 are the COM of helix X and the COM of the top (or bottom) half of helix X, and X3 is a selected Cα atom for defining ρ of helix X with respect to another. R is defined as a distance between A1 and B1. The dihedral angles of A2–A1–B1–B2 and A3–A2–A1–B1 are used to define Ω and ρ^{AB} for helix A with respect to helix B. In this work, a two-step procedure is applied; the first step is to simulate the association process, while the PMF at a target value of Ω, and ρ is calculated in the second step using a flat bottom harmonic restraint to prevent the TM helices from drifting away from each other. To obtain a 2d-PMF along with Ω, and ρ, about 500 independent US MD simulations were carried out. In Fig. 3b and c, the native-like right-handed dimer structures of GpA were observed in the 2d-PMF, when both $GBSW_{MEMB}$ and IMM1 implicit models were used in the simulation. As a second stable conformation, both simulations suggested a left-handed structure. The PMFs obtained by the 2d-US along with Ω and ρ were also compared to that obtained by T-REMD. At the same temperature (300 K), the two PMFs show good agreement regardless of the difference in sampling algorithms. At higher temperatures in T-REMD, a broader distribution along ρ was observed, while the distribution of Ω remained narrow. This was partially due to the flat bottom distance restraints in the T-REMD simulations.

There are only few simulation studies of the GpA dimer associations in explicit solvent and membranes, presumably due to the large computational cost. MD simulations based on the MARTINI CG models [73] and the PACE (hybrid all-atom protein/CG MARTINI lipid) models [49] successfully reproduced the GpA dimer structures in DPPC bilayers. Promisingly, the binding stability of the GpA dimer was estimated at around 10 kcal/mol regardless of the membrane models [72–74] in good agreement with the experimental value [197].

4.2. Phospholamban (PLN)

Phospholamban (PLN) is an integral membrane protein that consists of 52 amino acid residues (Table 1) [204]. It works as a reversible regulator protein for the activity of the sarcoplasmic/endoplasmic reticulum calcium pump (SERCA). The structure of PLN is composed of a cytoplasmic helix (residues 1–16), a TM helix (residues 22–52), and a linker region (residues 18–21) [205]. In membranes, PLN has a strong tendency to take oligomer forms, and the pentamer is known as the most stable oligomer. However, when PLN interacts with SERCA in membranes, PLN takes a monomeric form [206], suggesting that there is a dynamic equilibrium between monomer and pentamer forms [207]. The monomer structure of PLN was determined in detergent micelle (PDB ID: 1N7L) by solution NMR [205] and in a mixed bilayer (PDB ID: 2KB7) by solid-state NMR [208]. The pentamer structure in detergent micelles was first determined by solution NMR and is known as the 'bellflower' structure (PDB ID: 1ZLL) [209], where the cytoplasmic helix is greatly exposed in solution. Another pentamer structure determined by solid-state NMR showed that the cytoplasmic helix is partially embedded in the membranes ('pinwheel' structure) (PDB ID: 2KYV) [210]. The stabilities of these two pentamer structures were examined by using all-atom

Table 1
The amino acid sequences of the proteins discussed in this review.

Proteins	Amino acid sequence
Glycophorin A (GpA)	E_{72}ITLI TGVMA GVIGT ILLIS YGI_{95}
Phospholamban (PLN)	MEKVQ YLTRS AIRRA STIEM PQQAR QNLQN LFINF ALILI FLLLI AIIVM LL
Amyloid precursor protein (APP)	DAEFR HDSGY EVHHQ KLVFF AEDVG SNKGA IIGLM VGGVV ATVI VITLV MLKKK

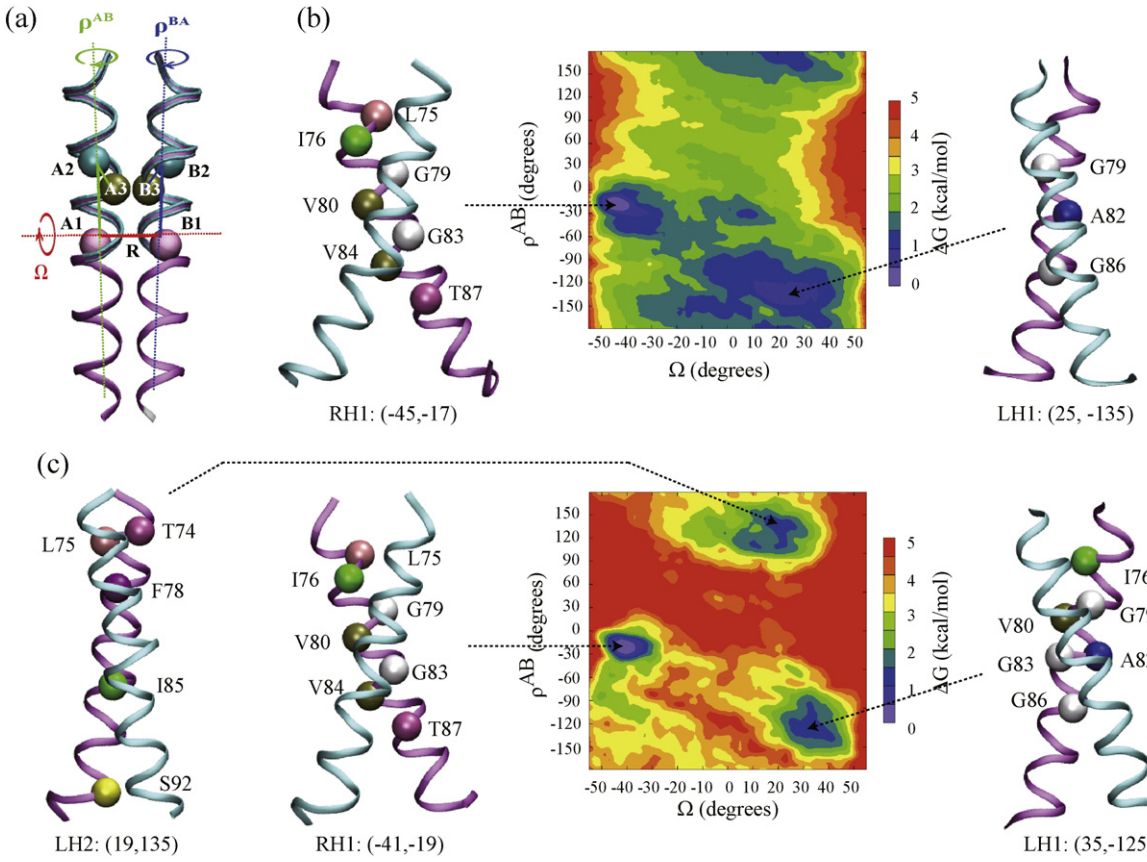

Fig. 3. MD simulations of GpA dimer. (a) The definition of interhelical distance (R), interhelical crossing angle (Ω), and relative rotational angle (ρ). (b) The potential of mean force (PMF) and two major dimer structures from T-REMD/IMM1 simulation. (c) PMF and three major dimer structures from T-REMD/GBSW$_{MEMB}$ simulation.
Reprinted with permission from [75]. Copyright 2014 John Wiley & Sons, Inc.

MD simulations in a lipid bilayer, and Kim et al. found that the cytoplasmic domain in the bellflower structure was highly unstable [78], suggesting that this structure is stable only in detergent micelle conditions.

The oligomer structures of PLN as well as GpA and the M2 proton channel (M2) were investigated by T-REMD simulations with the GBSW$_{MEMB}$ model [77]. In experiments, their most stable oligomer structures were known as a dimer (GpA), tetramer (M2), and pentamer (PLN). In the simulation, they utilized the IMAGE facility in CHARMM to simulate putative oligomers. In three cases, the simulations successfully predicted the native homo-oligomer structures, using only the native oligomerization state as a structural constraint. For PLN, they could predict the pentamer structure as the most stable oligomer without the constraint, while GpA and M2 were not predicted as a dimer and a tetramer state, presumably due to the insufficient parameterization of peptide–lipid dispersion interactions.

How PLN interacts with SERCA to regulate the ion uptake is the central question, yet it remains unresolved. Biochemical experiments showed that phosphorylation of PLN at Ser16 by cAMP-dependent protein kinase [211] or at Thr17 by Ca^{2+}/calmodulin-dependent kinase relieves the inhibition [212]. However, molecular mechanisms underlying the regulation remain elusive. Before the atomic structures of SERCA had been determined by X-ray crystallography, structural information was accumulated via S–S cross-linking experiments [213]. In 2003, Toyoshima et al. proposed a structural model of PLN bound to SERCA based on the E2-state crystal structure of SERCA and three distance restraints: (SERCA, PLN) = (L321, N27), (V89, V49), and (K397/K400, K3) [214]. Ten years later, an atomic structure of SERCA/PLN complex was determined at 2.8 Å resolution by X-ray crystallography [215]. The transmembrane interaction between SERCA and PLN is close to those in Toyoshima's model, while the cytoplasmic information is missing in the crystal structure due to the truncation of PLN.

The effect of phosphorylation at Ser16 was also investigated computationally by MD simulations [78], T-REMD in water [76], and T-REMD with the HDGB implicit membrane model to fully sample the dynamics of the flexible cytoplasmic domain at the membrane surface [80]. The simulation results suggested that phosphorylation at Ser16 increases the flexibility of PLN [76], and the simulation results are in good agreement with the experimental observation [216]. The PLN monomer was also simulated using T-REMD in the HDGB implicit membrane models with four different membrane thicknesses, again taking advantage of the implicit membrane to easily change the membrane thickness simply by changing the dielectric profile [79]. In thicker membranes, the population of T-shape structure, in which the cytoplasmic helix tightly interacts with membranes, increases, whereas the interhelical angle is greater in thinner membranes (Fig. 4). Since a thinner membrane may be representative of detergents such as $C_{12}E_8$, the simulations suggested that the fully extended conformation of PLN is sampled only in $C_{12}E_8$ detergent condition. Furthermore, this implies that the SS-crosslink between K397/K400 in SERCA and K3 in PLN is a result of the particular detergent that was used in the experiment.

4.3. Amyloid precursor protein (APP)

Alzheimer's disease (AD) causes dementia in many elderly people. Aggregation of amyloid β peptide (Aβ) in the brain is considered to be the primary element in the pathogenesis of AD [217]. In the initial process, amyloid precursor protein (APP), a type-I membrane protein, is cleaved on the extracellular β-site by β-secretase, which produces APP-C99, the remaining APP after the cleavage. γ-Secretase then cleaves the transmembrane γ-site (Gly_{38}–Thr_{43}), which produces Aβ peptides, primarily, $Aβ_{1-40}$ and $Aβ_{1-42}$ that aggregate in the later process [218–220].

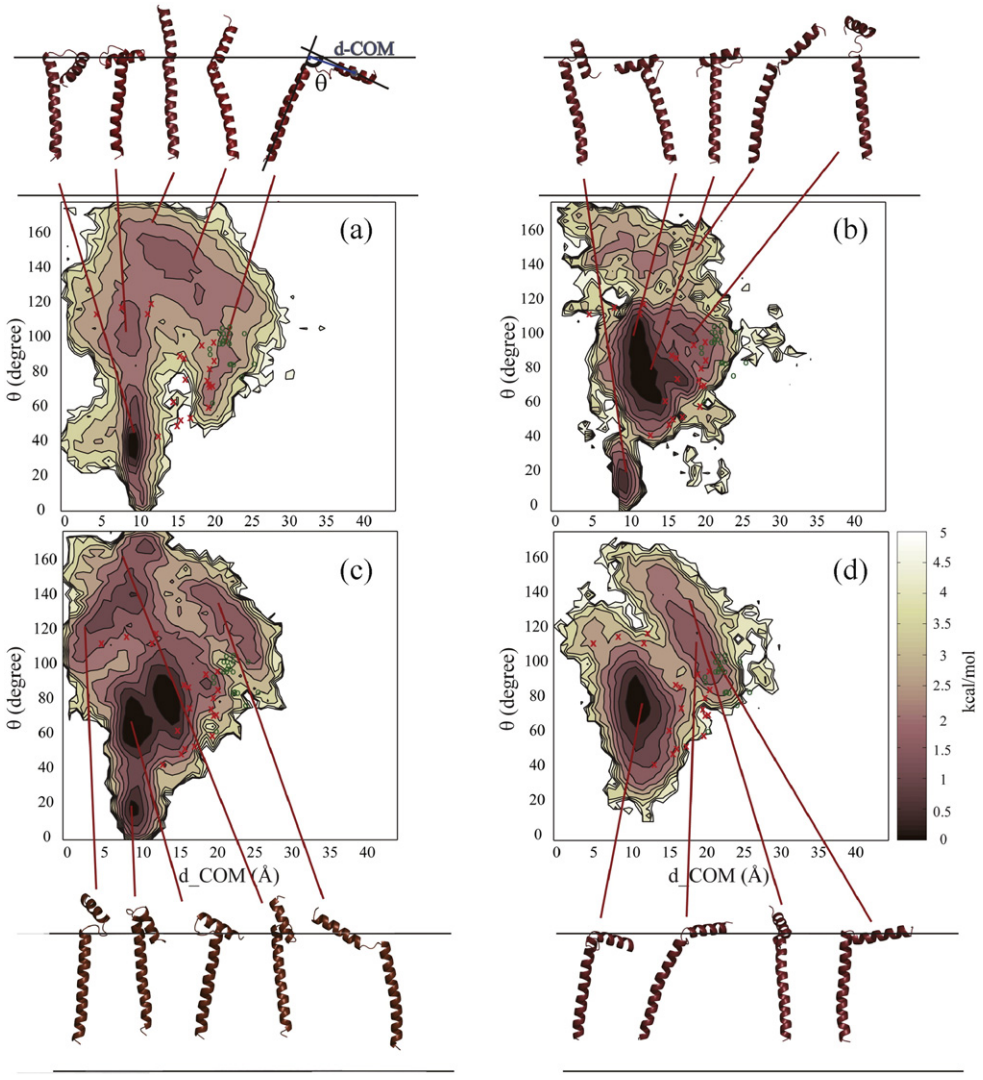

Fig. 4. Effect of membrane thickness in phospholamban monomer structures. Dielectric/nonpolar profile thicknesses in the HDGB implicit membrane models are (a) 24.5/24 Å, (b) 25.5/24 Å, (c) 26/26 Å, and (d) 26.5/27 Å, respectively.
Reprinted with permission from [79]. Copyright 2010, Biophysical Society.

Structural information on the TM domain of APP-C99 is important for understanding the molecular mechanisms underlying the Aβ production. Although its secondary structure was determined in 2008 [221] (Fig. 5a), the detailed atomic structure was not resolved. Miyashita et al. carried out T-REMD simulations of $A\beta_{1-40}$, $A\beta_{1-42}$, and $A\beta_{1-55}$ (or APP-$C99_{1-55}$) in the $GBSW_{MEMB}$ model to predict their structures [82]. $A\beta_{1-40}$ and $A\beta_{1-42}$ in a membrane environment take similar structure, in which two helical domains A(13-22), B(30-35), and a type I β-turn at 23-27 exist in a membrane interface. The transmembrane domain of APP-$C99_{1-55}$ consists of a helix kinked at Gly37–Gly38 ('GG-kink') (Fig. 5b). This structure is in good agreement with the solution NMR structure (PDB ID: 2LP1) and has been confirmed by all-atom membrane simulations [222]. Multi-scale simulations of APP-$C99_{15-55}$, where microsecond time scale CGMD simulations using MARTINI models were followed by 100-ns time-scale all-atom MD simulations using all-atom the CHARMM36 force field, confirmed the prediction by the T-REMD/$GBSW_{MEMB}$ simulations [83]. In particular, the NMR solution structure in micelle was in good agreement with the MD simulations in the same (detergent micelle) conditions [222] (Fig. 5c–e).

APP has three consecutive GxxxG motifs ($G_{25}xxxG_{29}xxxG_{33}xxxG_{38}$) in its juxtamembrane and TM regions. Munter et al. first suggested that $G_{29}xxxG_{33}$ plays a key role on the TM helix dimerization [223], whereas Kienlen-Campart et al. suggested that $G_{33}xxxG_{38}$ is the contact interface [224]. They also examined the effect of hydrophobic mutations at the $G_{33}xxxG_{38}$ motif, namely $L_{33}xxxL_{38}$ and $I_{33}xxxI_{38}$, on the APP dimerization. Although the mutation increases dimerization of APP TM domains, it leads to a drastic reduction of $A\beta_{1-40}$ and $A\beta_{1-42}$ secretion. To examine the ability of TM helix dimer in APP wild type and the difference of dimerization between wild type and $L_{33}xxxL_{38}$ mutant, Miyashita et al. carried out T-REMD simulations of the wild type APP and its $L_{33}xxxL_{38}$ mutant using the IMM1 model [81]. The simulations showed that the wild type APP forms a dimer via the backbone interaction at $G_{33}xxxG_{38}$ (Fig. 6a), as shown by Kielen-Campart et al., while the interface of the mutant APP is the hydrophobic sidechain interactions at $L_{33}xxxL_{38}$ (Fig. 6b). Interestingly, the γ-cleavage site of the mutant is shifted downward by 3 Å along the bilayer normal, suggesting that the mutation causes a mismatch between the γ-cleavage site in APP and the active site of γ-secretase, causing the reduction of $A\beta_{1-40}$ and $A\beta_{1-42}$ secretion.

In 2012, a dimer structure of APP TM domain in micelle environments was determined by solution NMR (Fig. 6c) [225]. In this structure, two $G_{33}xxxG_{38}$ motifs do not face each other, which contradict the previous experiment and simulations. Dominguez et al. performed again multi-scale simulations of an APP dimer (APP_{1-55}) in a DPC micelle and a POPC bilayer [84]. They carried out 50 individual 1.5-μs CGMD

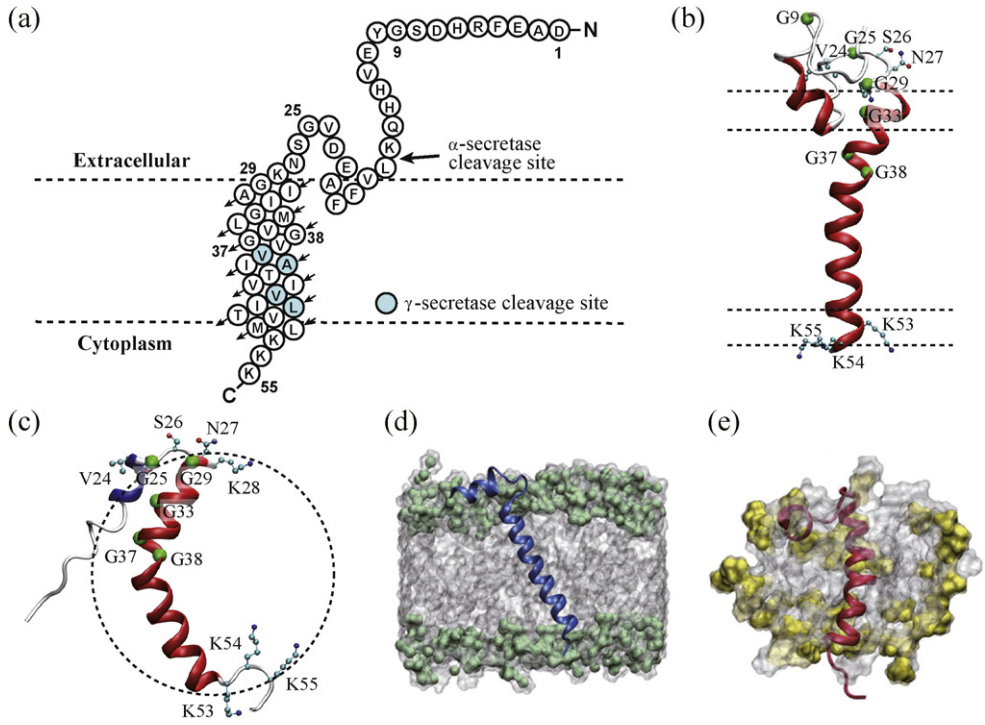

Fig. 5. The experimental and computational approaches for APP-C99 monomer structures. (a) The secondary structure information, (b) the predicted structure of APP-C99$_{1\text{-}55}$ by T-REMD/GBSW$_{MEMB}$ simulations, (c) the solution NMR structure in micelles, (d) the predicted structure of APP-C99$_{1\text{-}55}$ in a POPC bilayer, and (e) in DPC micelles by multi-scale approaches. For Fig. 5d and e, reprinted with permission from [83]. Copyright 2013, American Chemical Society.

simulations and a 100-ns all-atom MD simulation. Based on the relative rotational angles, they classified the APP TM dimer structures into three types: Gly-in, Gly-out, and Gly-side. In 'Gly-in', both of two $G_{33}xxxG_{38}$ face each other at the TM contact interface, whereas both of them face outsides in 'Gly-out'. In 'Gly-side', only one $G_{33}xxxG_{38}$ faces inside while the other faces outside. The simulations suggested that Gly-in is

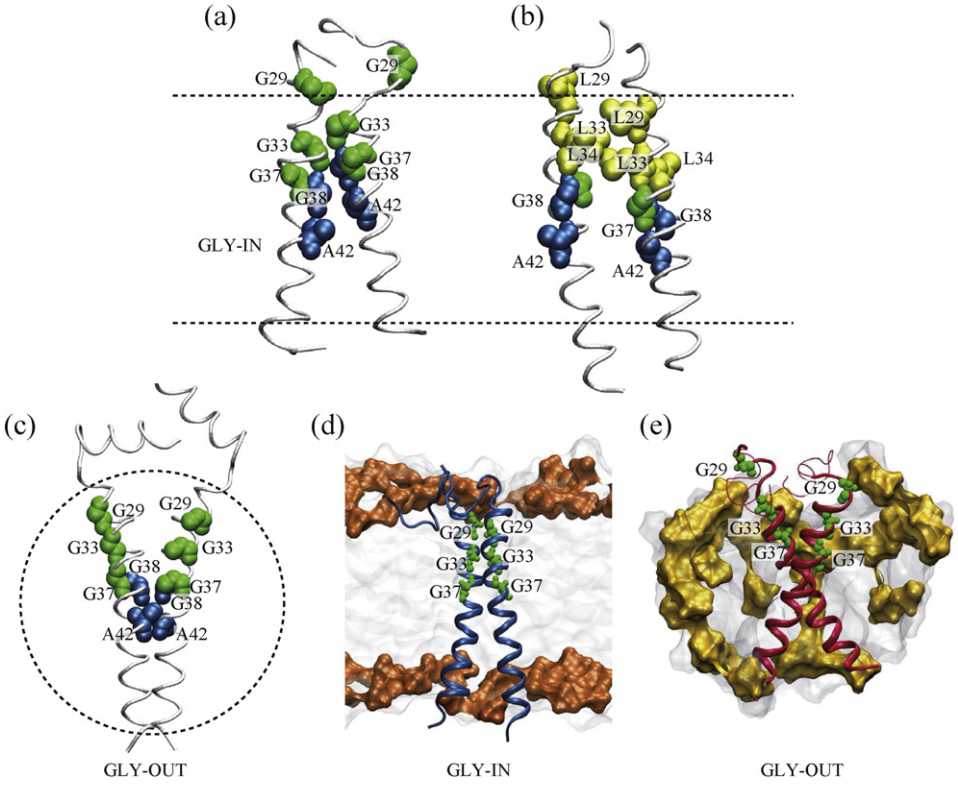

Fig. 6. The experimental and computational approaches for APP dimer structures. (a) The predicted structure of wild type APP-C99$_{1\text{-}55}$, (b) $L_{33}xxxL_{38}$ mutant structure by T-REMD/IMM1 simulations, (c) the solution NMR structure in micelles, (d) the predicted structure of APP-C99$_{1\text{-}55}$ in a POPC bilayer, and (e) in DPC micelles by multi-scale simulations. For Fig. 6d and e, reprinted with permission from [84]. Copyright 2014, American Chemical Society.

the most stable TM helix dimer structure in a POPC lipid bilayer (Fig. 6d), while Gly-out and Gly-side are dominant in micelle environments (Fig. 6e). This result agrees with all the experimental and simulation results, suggesting that a membrane environment greatly affects the dimer structure of APP.

4.4. Mixed lipid bilayers

Mixed lipid systems are the major structural component of biological membranes. They are involved in a number of cellular processes like signal transduction, membrane trafficking, and immune responses. However, it is difficult to predict membrane structures with multiple components, because lateral diffusion of lipid molecules is very slow (10^{-9}–10^{-7} cm^2 s^{-1}) and it takes longer time to obtain an equilibrated structure in all-atom MD simulation [226]. Thus, enhanced sampling methods can play an important role in studying such heterogeneous bilayer systems.

Wang et al. examined acceleration of lateral diffusion and mixing of two lipid components by using the aMD method [85]. In their method, the dihedral potential was boosted, which enhances *trans-gauche* isomerization of lipid acyl chains during the simulation. They simulated mixed POPC/DMPC lipid bilayers from a state in which two lipid phases are completely separated, and analyzed structural change of lipid molecules as well as lipid lateral diffusion. They found that in aMD, *trans-gauche* isomerization occurred 7.7- and 5.3-fold faster in POPC and DMPC, respectively, compared to the conventional MD. In addition, aMD showed two- to three-fold speedup in lipid mixing. They also suggested that E_{cut} and α in the boost potential is important to determine the speedup in lipid lateral diffusion. Increasing E_{cut} was especially effective for enhancing the diffusion. Changing α affects structural change of acyl chains in POPC rather than DMPC.

REST simulations were also applied to a mixed lipid bilayer system for a similar purpose by Huang and Garcia [86]. The simulation system contained 144 DPPC, 144 cholesterol, and ~14,000 water molecules. DPPC lipids were chosen as the tempered solute. They estimated that 12 replicas are enough in REST to cover the same temperature range (323 to 600 K) with T-REMD, while full T-REMD needs ~100 replicas. In the REST simulations, they found that lipid lateral diffusion is enhanced by an order of magnitude compared to the conventional MD, and observed faster convergence in the radial distribution function of cholesterol. They suggested that REST is useful for investigating membrane lateral heterogeneity.

Mori et al. simulated mixed POPC/DMPC bilayers by using γT-REMD, T-REMD, γ-REMD, and MD simulations, and examined the effect of the surface tension on the membrane structures with multiple components [87]. In their simulations, they observed that some replicas in γT-REMD showed accelerated mixing of two lipids compared to MD (Fig. 7a). They analyzed the mean–square displacement of POPC and DMPC, and found that all REMD simulations showed accelerated lipid lateral diffusion but the degree to which acceleration was achieved followed the following order: T-REMD > γT-REMD > γ-REMD > MD (Fig. 7b). The enhanced lateral diffusion in T-REMD is simply due to high temperature, and those in γ-REMD are due to free-area effects. Since diffusion and mixing are actually not identical in the mixed lipid-bilayer systems, they also quantified the degree of mixing of two lipid components by analyzing the number of contact pairs between POPC and DMPC (Fig. 7c). They found that mixing was enhanced in T-REMD compared to MD, while it was suppressed in γ-REMD. In γT-REMD, both enhancement and suppression were observed, presumably because mixing is accelerated at high temperature while it is suppressed under high surface tension. From these enhanced sampling simulations, they concluded that surface tension suppresses mixing of two lipid components, while temperature has the opposite effect.

5. Conclusions and perspectives

We have reviewed various molecular models and enhanced conformational sampling algorithms for biomembrane simulations and contrasted their advantages and disadvantages. For example, the GB models offer significant advantages for studying the dynamics of

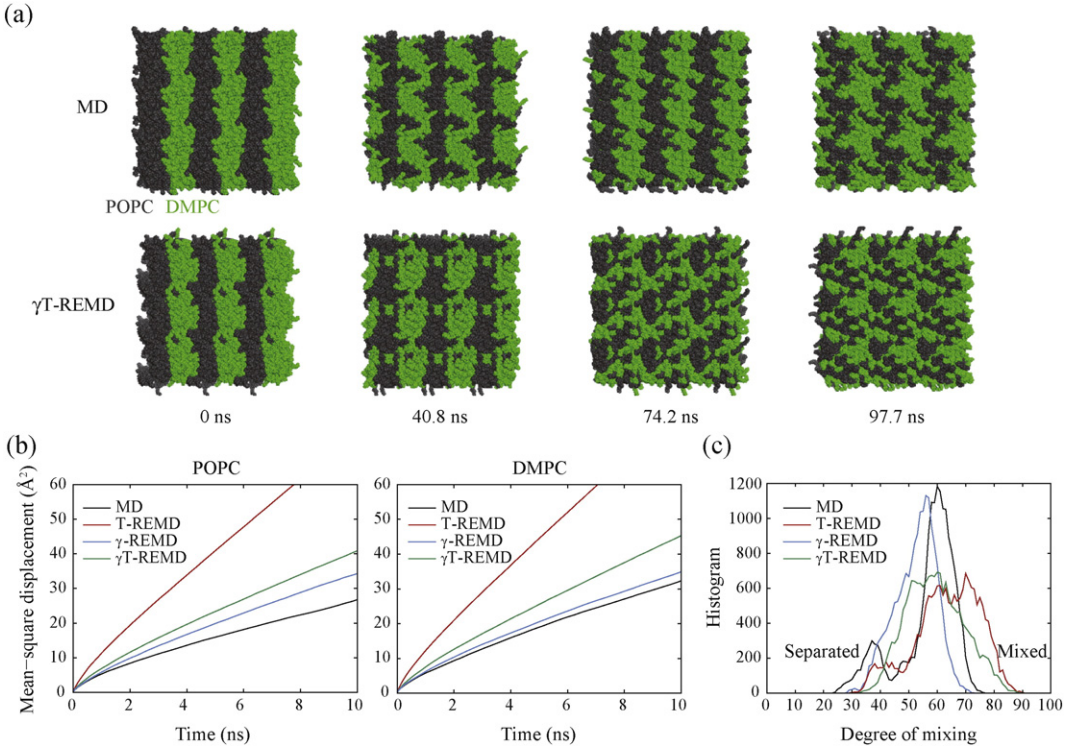

Fig. 7. Mixing of lipids by different REMD methods. (a) Snapshots in the conventional MD simulation (top) and the γT-REMD (bottom). (b) Mean square displacement of POPC and DMPC molecules as a function of time, (c) histogram of degree of mixing (see the details in the original article).
For Figs. 7b and c, reprinted with permission from [87]. Copyright 2015, Wiley.

membrane embedded proteins, especially in combination with REMD, but they are the most useful for relatively small molecules, where the computational advantage over explicit solvent models is greatest. Furthermore, the GB models may miss functionally relevant specific interactions between protein and solvent. With respect to enhanced sampling methods, the REMD methods do not need empirical parameters, but many replicas are required for explicit solvent systems, and sampling is not guided in a specific way to overcome system barriers. REUS targets barriers more specifically, but needs appropriate reaction coordinates to compute the free energy landscape in a complex system. REST can reduce the number of replicas in explicit solvent simulations, while scaling of protein–protein interactions may generate unnatural protein structures in high temperature replicas. Finally, aMD is less straightforward to use because it requires trial-and-error optimization to obtain reasonable parameters (E_{cut} and α) for effective accelerated conformational sampling. The enhanced sampling schemes also vary in the requirement of large parallel computer resources when many replica simulations have to be run simultaneously.

We would like to briefly introduce two other important algorithms for biomembrane simulations. One is the use of reaction path method, like the string method [227]. Moradi et al. extensively searched a number of pathways that describe large conformational changes of membrane transporters by multiple targeted MD simulations [228]. Using the pathway whose free-energy change is smaller than other ones, they refined the conformational transition pathway by applying the string method. Finally, they carried out REUS (or bias-exchange MD) using the collective variables that can describe the transition pathway. This approach is a promising way for simulating conformational changes of large membrane proteins. So far, ABC transporter and glycerol-3-phosphate:phosphate antiporter were simulated by this approach for understanding not only the conformational changes [229] but also the free-energy profiles upon the ligand-induced conformational changes [230]. Another important work is the use of Markov state model (MSM) for long-timescale processes from large number of independent MD simulations [231]. MSM has been used to understand protein folding, conformational change, and protein–ligand docking [232]. Recently, Kohlhoff et al. applied this method to explore ligand modulation of GPCR activation pathways [233]. They carried out tens of thousands of individual ~10-ns MD simulations of β_2AR in explicit solvent and membrane, and found that the activation of β_2AR takes place along multiple pathways consisting of metastable intermediate states.

As illustrated with the recent simulation studies of GpA, PLN, and APP, the implicit models can be combined successfully with T-REMD or REUS to enhance conformational sampling. The advantage of this approach is that one could examine physical properties of membranes or protein/membrane interactions using relatively modest computational resources. The predicted GpA, PLN, and APP structures by this approach compare favorably with experiment, suggesting that the model and simulation approaches are sufficiently accurate. The next challenge would be the application to the study of dynamics in larger membrane proteins where there are many unresolved questions, in particular with respect to membrane protein association, membrane protein folding, membrane protein–ligand binding interaction, large conformational changes of membrane transporter, and other topics. The extensive use of GPUs is a key step for such applications requiring that implicit membrane models and enhanced sampling schemes are implemented efficiently on such platforms.

The enhanced mixing of lipids with T-REMD, REST, and aMD is a benefit for explicit lipid/solvent simulations but the large degrees of freedom in systems where large proteins are embedded in explicit bilayers greatly increase the number of replicas, especially in the T-REMD scheme. In some of those cases, the use of aMD may be a good alternative, since aMD requires less computational resources compared to the other methods as evidenced in several recent publications where the conformational changes of membrane proteins were enhanced by this method [234,235]. On the other hand, T-REMD simulations of large membrane proteins may not be practical in near future. However, similar to an approach taken by the Straub's group for studying APP [81–84], multi-scale simulations combined with T-REMD/Implicit solvent, CGMD, and all-atom MD may be a good strategy for tackling complex biological phenomena like membrane protein folding.

We expect that advanced computational methods that take advantage of enhanced sampling and/or efficient representations of membrane environments will continue to explore increasingly wider conformational space to drive and complement experiments with the ultimate goal of fully understand relationships between structure, dynamics, and function of membrane proteins.

Transparency document

The Transparency document associated with this article can be found, in online version.

Acknowledgments

MF, WI, and YS thank many colleagues who have helped us to carry out biomembrane simulations. In particular, we are grateful to Charlie Brooks and Yuko Okamoto for their supports in our early carriers for development of implicit solvent and membrane models as well as the generalized-ensemble simulations. We also thank the young scientists who carried out extensive biomembrane simulation studies in each of our research groups (Pai-Chi Li, Yumi Kashihara (with YS), Soohyung Park (with WI), Maryam Sayadi, Afra Panahi, Seiichiro Tanizaki (with MF)). YS also acknowledge to Chikashi Toyoshima and Mitsunori Ikeguchi for collaboration on Phospholamban, as well as John Straub and Dave Thirumalai for collaboration on Amyloid precursor proteins.

This research used the computational resources of K computer provided by the RIKEN Advanced Institute for Computational Science through the HPCI System Research project (Project ID: ra000009, hp120060, hp120309, hp130003, hp140091, hp140169, and hp140229) (to YS and TM), TSUBAME2.5 at the Tokyo Institute of Technology through the HPCI System Research Project (project ID hp150060) (to TM), the RIKEN Integrated Cluster of Clusters (RICC) at RIKEN (to YS), HOKUSAI GreatWave at RIKEN (to TM), and XSEDE MCB070009 (to WI), and XSEDE MCB090003 (to MF).

This research was supported in part by a Grant-in-Aid for Scientific Research on Innovative Areas (No. 26119006) and the fund from the High Performance Computing Infrastructure (HPCI) Strategic Program of the Ministry of Education, Culture, Sports, Science and Technology (MEXT) (to YS), a Grant-in-Aid for Young Scientists (A) from MEXT/JSPS KAKENHI (No. 15H05594) (to TM), NSF MCB-1157677, NIH GM092950, and NIH U54GM087519 (to WI), NIH GM092949, NIH GM084953, NSF MCB 1330560, and NSF CBET 0941055 (to MF).

References

[1] G.L. Nicolson, The fluid-mosaic model of membrane structure: still relevant to understanding the structure, function and dynamics of biological membranes after more than 40 years, Biochim. Biophys. Acta Biomembr. 1838 (2014) 1451–1466.
[2] J.F. Nagle, S. Tristram-Nagle, Structure of lipid bilayers, Biochim. Biophys. Acta Rev. Biomembr. 1469 (2000) 159–195.
[3] T. Tsukazaki, H. Mori, S. Fukai, R. Ishitani, T. Mori, N. Dohmae, A. Perederina, Y. Sugita, D.G. Vassylyev, K. Ito, O. Nureki, Conformational transition of Sec machinery inferred from bacterial SecYE structures, Nature 455 (2008) 988–992.
[4] L.G. Cuello, V. Jogini, D.M. Cortes, A.C. Pan, D.G. Gagnon, O. Dalmas, J.F. Cordero-Morales, S. Chakrapani, B. Roux, E. Perozo, Structural basis for the coupling between activation and inactivation gates in K^+ channels, Nature 466 (2010) 272–275.
[5] R. Kanai, H. Ogawa, B. Vilsen, F. Cornelius, C. Toyoshima, Crystal structure of a Na^+-bound Na^+,K^+-ATPase preceding the E1P state, Nature 502 (2013) 201–206.
[6] Y. Xu, Y.Y. Tao, L.S. Cheung, C. Fan, L.Q. Chen, S. Xu, K. Perry, W.B. Frommer, L. Feng, Structures of bacterial homologues of SWEET transporters in two distinct conformations, Nature 515 (2014) 448–452.
[7] D.M. Rosenbaum, S.G.F. Rasmussen, B.K. Kobilka, The structure and function of G-protein-coupled receptors, Nature 459 (2009) 356–363.

[8] S.K. Shenoy, R.J. Lefkowitz, β-Arrestin-mediated receptor trafficking and signal transduction, Trends Pharmacol. Sci. 32 (2011) 521–533.
[9] B.P. Head, H.H. Patel, P.A. Insel, Interaction of membrane/lipid rafts with the cytoskeleton: impact on signaling and function membrane/lipid rafts, mediators of cytoskeletal arrangement and cell signaling, Biochim. Biophys. Acta Biomembr. 1838 (2014) 532–545.
[10] S.H. White, The progress of membrane protein structure determination, Protein Sci. 13 (2004) 1948–1949.
[11] D. Kozma, I. Simon, G.E. Tusnady, PDBTM: protein data bank of transmembrane proteins after 8 years, Nucleic Acids Res. 41 (2013) D524–D529.
[12] C. Toyoshima, F. Cornelius, New crystal structures of PII-type ATPases: excitement continues, Curr. Opin. Struct. Biol. 23 (2013) 507–514.
[13] F. Khalili-Araghi, J. Gumbart, P.C. Wen, M. Sotomayor, E. Tajkhorshid, K. Schulten, Molecular dynamics simulations of membrane channels and transporters, Curr. Opin. Struct. Biol. 19 (2009) 128–137.
[14] P.J. Stansfeld, M.S.P. Sansom, Molecular simulation approaches to membrane proteins, Structure 19 (2011) 1562–1572.
[15] R.O. Dror, R.M. Dirks, J.P. Grossman, H.F. Xu, D.E. Shaw, Biomolecular simulation: a computational microscope for molecular biology, Annu. Rev. Biophys. 41 (2012) 429–452.
[16] Z. Cournia, T.W. Allen, I. Andricioaei, B. Antonny, D. Baum, G. Brannigan, N.V. Buchete, J.T. Deckman, L. Delemotte, C. del Val, R. Friedman, P. Gkeka, H.C. Hege, J. Henin, M.A. Kasimova, A. Kolocouris, M.L. Klein, S. Khalid, M.J. Lemieux, N. Lindow, M. Roy, J. Selent, M. Tarek, F. Tofoleanu, S. Vanni, S. Urban, D.J. Wales, J.C. Smith, A.N. Bondar, Membrane protein structure, function, and dynamics: a perspective from experiments and theory, J. Membr. Biol. 248 (2015) 611–640.
[17] K. Arora, C.L. Brooks, Functionally important conformations of the Met20 loop in dihydrofolate reductase are populated by rapid thermal fluctuations, J. Am. Chem. Soc. 131 (2009) 5642–5647.
[18] J.I. Sulkowska, J.K. Noel, J.N. Onuchic, Energy landscape of knotted protein folding, Proc. Natl. Acad. Sci. U. S. A. 109 (2012) 17783–17788.
[19] K. Nam, J.Z. Pu, M. Karplus, Trapping the ATP binding state leads to a detailed understanding of the F_1-ATPase mechanism, Proc. Natl. Acad. Sci. U. S. A. 111 (2014) 17851–17856.
[20] R.L. Hayes, J.K. Noel, U. Mohanty, P.C. Whitford, S.P. Hennelly, J.N. Onuchic, K.Y. Sanbonmatsu, Magnesium fluctuations modulate RNA dynamics in the SAM-I riboswitch, J. Am. Chem. Soc. 134 (2012) 12043–12053.
[21] A. Yildirim, M. Sharma, B.M. Varner, L. Fang, M. Feig, Conformational preferences of DNA in reduced dielectric environments, J. Phys. Chem. B 118 (2014) 10874–10881.
[22] J. Panecka, M. Havrila, K. Reblova, J. Sponer, J. Trylska, Role of S-turn2 in the structure, dynamics, and function of mitochondrial ribosomal A-site. A bioinformatics and molecular dynamics simulation study, J. Phys. Chem. B 118 (2014) 6687–6701.
[23] V. Gapsys, B.L. de Groot, R. Briones, Computational analysis of local membrane properties, J. Comput. Aided Mol. Des. 27 (2013) 845–858.
[24] H.I. Ingolfsson, M.N. Melo, F.J. van Eerden, C. Arnarez, C.A. Lopez, T.A. Wassenaar, X. Periole, A.H. de Vries, D.P. Tieleman, S.J. Marrink, Lipid organization of the plasma membrane, J. Am. Chem. Soc. 136 (2014) 14554–14559.
[25] Z.A. Levine, R.M. Venable, M.C. Watson, M.G. Lerner, J.E. Shea, R.W. Pastor, F.L.H. Brown, Determination of biomembrane bending moduli in fully atomistic simulations, J. Am. Chem. Soc. 136 (2014) 13582–13585.
[26] A.J. Sodt, M.L. Sandar, K. Gawrisch, R.W. Pastor, E. Lyman, The molecular structure of the liquid-ordered phase of lipid bilayers, J. Am. Chem. Soc. 136 (2014) 725–732.
[27] R. Kadirvelraj, O.C. Grant, I.J. Goldstein, H.C. Winter, H. Tateno, E. Fadda, R.J. Woods, Structure and binding analysis of polyporus squamosus lectin in complex with the Neu5Acα2-6Galβ1-4GlcNAc human-type influenza receptor, Glycobiology 21 (2011) 973–984.
[28] W. Nishima, N. Miyashita, Y. Yamaguchi, Y. Sugita, S. Re, Effect of bisecting GlcNAc and core fucosylation on conformational properties of biantennary complex-type N-glycans in solution, J. Phys. Chem. B 116 (2012) 8504–8512.
[29] H.S. Lee, Y.F. Qi, W. Im, Effects of N-glycosylation on protein conformation and dynamics: protein data bank analysis and molecular dynamics simulation study, Sci. Rep. 5 (2015) 8926.
[30] S.J. Marrink, H.J.C. Berendsen, Simulation of water transport through a lipid–membrane, J. Phys. Chem. 98 (1994) 4155–4168.
[31] S.E. Feller, R.M. Venable, R.W. Pastor, Computer simulation of a DPPC phospholipid bilayer: structural changes as a function of molecular surface area, Langmuir 13 (1997) 6555–6561.
[32] P.B. Moore, C.F. Lopez, M.L. Klein, Dynamical properties of a hydrated lipid bilayer from a multinanosecond molecular dynamics simulation, Biophys. J. 81 (2001) 2484–2494.
[33] E.L. Wu, P.J. Fleming, M.S. Yeom, G. Widmalm, J.B. Klauda, K.G. Fleming, W. Im, *E. coli* outer membrane and interactions with OmpLA, Biophys. J. 106 (2014) 2493–2502.
[34] E.L. Wu, Y.F. Qi, S. Park, S.S. Mallajosyula, A.D. MacKerell, J.B. Klauda, W. Im, Insight into early-stage unfolding of GPI-anchored human prion protein, Biophys. J. 109 (2015) 2090–2100.
[35] A. Grossfield, M.C. Pitman, S.E. Feller, O. Soubias, K. Gawrisch, Internal hydration increases during activation of the G-protein-coupled receptor rhodopsin, J. Mol. Biol. 381 (2008) 478–486.
[36] R.O. Dror, D.H. Arlow, D.W. Borhani, M.O. Jensen, S. Piana, D.E. Shaw, Identification of two distinct inactive conformations of the β_2-adrenergic receptor reconciles structural and biochemical observations, Proc. Natl. Acad. Sci. U. S. A. 106 (2009) 4689–4694.
[37] D.E. Shaw, R.O. Dror, J.K. Salmon, J.P. Grossman, K.M. Mackenzie, J.A. Bank, C. Young, M.M. Deneroff, B. Batson, K.J. Bowers, E. Chow, M.P. Eastwood, D.J. Ierardi, J.L. Klepeis, J.S. Kuskin, R.H. Larson, K. Lindorff-Larsen, P. Maragakis, M.A. Moraes, S. Piana, Y. Shan, B. Towles, Millisecond-scale molecular dynamics simulations on Anton, International Conference for High Performance Computing, Networking, Storage and Analysis (SC09), Portland Oregon, USA, 2009.
[38] D.E. Shaw, J.A. Bank, B. Batson, J.A. Butts, J.C. Chao, M.M. Deneroff, R.O. Dror, A. Even, C.H. Fenton, A. Forte, J. Gagliardo, G. Gill, B. Greskamp, C.R. Ho, D.J. Ierardi, L. Iserovich, J.S. Kuskin, R.H. Larson, T. Layman, L.-S. Lee, A.K. Lerer, C. Li, D. Killebrew, K.M. Mackenzie, S.Y.-H. Mok, M.A. Moraes, R. Mueller, L.J. Nociolo, J.L. Peticolas, T. Quan, D. Ramot, J.K. Salmon, D.P. Scarpazza, U.B. Schafer, N. Siddique, C.W. Snyder, J. Spengler, P.T.P. Tang, M. Theobald, H. Toma, B. Towles, B. Vitale, S.C. Wang, C. Young, Anton 2: raising the bar for performance and programmability in a special-purpose molecular dynamics supercomputer, International Conference for High Performance Computing, Networking, Storage and Analysis (SC14), New Orleans, Louisiana, USA, 2014.
[39] M.O. Jensen, V. Jogini, D.W. Borhani, A.E. Leffler, R.O. Dror, D.E. Shaw, Mechanism of voltage gating in potassium channels, Science 336 (2012) 229–233.
[40] R.O. Dror, H.F. Green, C. Valant, D.W. Borhani, J.R. Valcourt, A.C. Pan, D.H. Arlow, M. Canals, J.R. Lane, R. Rahmani, J.B. Baell, P.M. Sexton, A. Christopoulos, D.E. Shaw, Structural basis for modulation of a G-protein-coupled receptor by allosteric drugs, Nature 503 (2013) 295–299.
[41] J.C. Gumbart, I. Teo, B. Roux, K. Schulten, Reconciling the roles of kinetic and thermodynamic factors in membrane–protein insertion, J. Am. Chem. Soc. 135 (2013) 2291–2297.
[42] C. Boiteux, I. Vorobyov, R.J. French, C. French, V. Yarov-Yarovoy, T.W. Allen, Local anesthetic and antiepileptic drug access and binding to a bacterial voltage-gated sodium channel, Proc. Natl. Acad. Sci. U. S. A. 111 (2014) 13057–13062.
[43] J.B. Klauda, R.M. Venable, J.A. Freites, J.W. O'Connor, D.J. Tobias, C. Mondragon-Ramirez, I. Vorobyov, A.D. MacKerell Jr., R.W. Pastor, Update of the CHARMM all-atom additive force field for lipids: validation on six lipid types, J. Phys. Chem. B 114 (2010) 7830–7843.
[44] J.P.M. Jambeck, A.P. Lyubartsev, An extension and further validation of an all-atomistic force field for biological membranes, J. Chem. Theory Comput. 8 (2012) 2938–2948.
[45] C.J. Dickson, B.D. Madej, A.A. Skjevik, R.M. Betz, K. Teigen, I.R. Gould, R.C. Walker, Lipid14: the amber lipid force field, J. Chem. Theory Comput. 10 (2014) 865–879.
[46] L. Saiz, M.L. Klein, Computer simulation studies of model biological membranes, Acc. Chem. Res. 35 (2002) 482–489.
[47] S.J. Marrink, H.J. Risselada, S. Yefimov, D.P. Tieleman, A.H. de Vries, The MARTINI force field: coarse grained model for biomolecular simulations, J. Phys. Chem. B 111 (2007) 7812–7824.
[48] Q. Shi, S. Izvekov, G.A. Voth, Mixed atomistic and coarse-grained molecular dynamics: simulation of a membrane-bound ion channel, J. Phys. Chem. B 110 (2006) 15045–15048.
[49] C.K. Wan, W. Han, Y.D. Wu, Parameterization of PACE force field for membrane environment and simulation of helical peptides and helix–helix association, J. Chem. Theory Comput. 8 (2012) 300–313.
[50] P. Kar, S.M. Gopal, Y.M. Cheng, A. Panahi, M. Feig, Transferring the PRIMO coarse-grained force field to the membrane environment: simulations of membrane proteins and helix–helix association, J. Chem. Theory Comput. 10 (2014) 3459–3472.
[51] D. Bashford, D.A. Case, Generalized Born models of macromolecular solvation effects, Annu. Rev. Phys. Chem. 51 (2000) 129–152.
[52] W. Im, J. Chen, C.L. Brooks, Peptide and protein folding and conformational equilibria: theoretical treatment of electrostatics and hydrogen bonding with implicit solvent models, Adv. Protein Chem. 72 (2006) 173–198.
[53] S.J. Marrink, D.P. Tieleman, Perspective on the Martini model, Chem. Soc. Rev. 42 (2013) 6801–6822.
[54] R.C. Bernardi, M.C.R. Melo, K. Schulten, Enhanced sampling techniques in molecular dynamics simulations of biological systems, Biochim. Biophys. Acta Gen. Subj. 1850 (2015) 872–877.
[55] A. Mitsutake, Y. Sugita, Y. Okamoto, Generalized-ensemble algorithms for molecular simulations of biopolymers, Biopolymers 60 (2001) 96–123.
[56] B.A. Berg, T. Neuhaus, Multicanonical ensemble: a new approach to simulate first-order phase-transitions, Phys. Rev. Lett. 68 (1992) 9–12.
[57] U.H.E. Hansmann, Y. Okamoto, Generalized-ensemble Monte Carlo method for systems with rough energy landscape, Phys. Rev. E 56 (1997) 2228–2233.
[58] G.H. Wei, A.I. Jewett, J.E. Shea, Structural diversity of dimers of the Alzheimer amyloid-β(25-35) peptide and polymorphism of the resulting fibrils, Phys. Chem. Chem. Phys. 12 (2010) 3622–3629.
[59] S. Cote, R. Laghaei, P. Derreumaux, N. Mousseau, Distinct dimerization for various alloforms of the amyloid-β protein: Aβ(1-40), Aβ(1-42), and Aβ(1-40)(D23N), J. Phys. Chem. B 116 (2012) 4043–4055.
[60] S.G. Itoh, H. Okumura, Hamiltonian replica-permutation method and its applications to an alanine dipeptide and amyloid-β(29-42) peptides, J. Comput. Chem. 34 (2013) 2493–2497.
[61] H.F. Lou, R.I. Cukier, Molecular dynamics of apo-adenylate kinase: a distance replica exchange method for the free energy of conformational fluctuations, J. Phys. Chem. B 110 (2006) 24121–24137.
[62] W. Im, C.L. Brooks, De novo folding of membrane proteins: an exploration of the structure and NMR properties of the fd coat protein, J. Mol. Biol. 337 (2004) 513–519.
[63] W. Im, C.L. Brooks, Interfacial folding and membrane insertion of designed peptides studied by molecular dynamics simulations, Proc. Natl. Acad. Sci. U. S. A. 102 (2005) 6771–6776.
[64] H. Nymeyer, T.B. Woolf, A.E. Garcia, Folding is not required for bilayer insertion: replica exchange simulations of an α-helical peptide with an explicit lipid bilayer, Proteins 59 (2005) 783–790.

[65] L. Wang, B.J. Berne, R.A. Friesner, On achieving high accuracy and reliability in the calculation of relative protein–ligand binding affinities, Proc. Natl. Acad. Sci. U. S. A. 109 (2012) 1937–1942.
[66] H. Kokubo, T. Tanaka, Y. Okamoto, Two-dimensional replica-exchange method for predicting protein–ligand binding structures, J. Comput. Chem. 34 (2013) 2601–2614.
[67] Y. Sugita, Y. Okamoto, Replica-exchange molecular dynamics method for protein folding, Chem. Phys. Lett. 314 (1999) 141–151.
[68] Y. Sugita, A. Kitao, Y. Okamoto, Multidimensional replica-exchange method for free-energy calculations, J. Chem. Phys. 113 (2000) 6042–6051.
[69] T. Mori, J. Jung, Y. Sugita, Surface-tension replica-exchange molecular dynamics method for enhanced sampling of biological membrane systems, J. Chem. Theory Comput. 9 (2013) 5629–5640.
[70] P. Liu, B. Kim, R.A. Friesner, B.J. Berne, Replica exchange with solute tempering: a method for sampling biological systems in explicit water, Proc. Natl. Acad. Sci. U. S. A. 102 (2005) 13749–13754.
[71] D. Hamelberg, J. Mongan, J.A. McCammon, Accelerated molecular dynamics: a promising and efficient simulation method for biomolecules, J. Chem. Phys. 120 (2004) 11919–11929.
[72] J. Henin, A. Pohorille, C. Chipot, Insights into the recognition and association of transmembrane α-helices. The free energy of α-helix dimerization in glycophorin A, J. Am. Chem. Soc. 127 (2005) 8478–8484.
[73] D. Sengupta, S.J. Marrink, Lipid-mediated interactions tune the association of glycophorin A helix and its disruptive mutants in membranes, Phys. Chem. Chem. Phys. 12 (2010) 12987–12996.
[74] S. Park, W. Im, Two dimensional window exchange umbrella sampling for transmembrane helix assembly, J. Chem. Theory Comput. 9 (2013) 13–17.
[75] P.C. Li, N. Miyashita, W. Im, S. Ishido, Y. Sugita, Multidimensional umbrella sampling and replica-exchange molecular dynamics simulations for structure prediction of transmembrane helix dimers, J. Comput. Chem. 35 (2014) 300–308.
[76] Y. Sugita, N. Miyashita, T. Yoda, M. Ikeguchi, C. Toyoshima, Structural changes in the cytoplasmic domain of phospholamban by phosphorylation at Ser16: a molecular dynamics study, Biochemistry 45 (2006) 11752–11761.
[77] L.T. Bu, W. Im, L.I. Charles, Membrane assembly of simple helix homo-oligomers studied via molecular dynamics simulations, Biophys. J. 92 (2007) 854–863.
[78] T. Kim, J. Lee, W. Im, Molecular dynamics studies on structure and dynamics of phospholamban monomer and pentamer in membranes, Proteins 76 (2009) 86–98.
[79] M. Sayadi, S. Tanizaki, M. Feig, Effect of membrane thickness on conformational sampling of phospholamban from computer simulations, Biophys. J. 98 (2010) 805–814.
[80] M. Sayadi, M. Feig, Role of conformational sampling of Ser16 and Thr17-phosphorylated phospholamban in interactions with SERCA, Biochim. Biophys. Acta Biomembr. 1828 (2013) 577–585.
[81] N. Miyashita, J.E. Straub, D. Thirumalai, Y. Sugita, Transmembrane structures of amyloid precursor protein dimer predicted by replica-exchange molecular dynamics simulations, J. Am. Chem. Soc. 131 (2009) 3438–3439.
[82] N. Miyashita, J.E. Straub, D. Thirumalai, Structures of β-amyloid peptide 1-40, 1-42, and 1-55-the 672-726 fragment of APP-in a membrane environment with implications for interactions with γ-secretase, J. Am. Chem. Soc. 131 (2009) 17843–17852.
[83] L. Dominguez, S.C. Meredith, J.E. Straub, D. Thirumalai, Transmembrane fragment structures of amyloid precursor protein depend on membrane surface curvature, J. Am. Chem. Soc. 136 (2014) 854–857.
[84] L. Dominguez, L. Foster, S.C. Meredith, J.E. Straub, D. Thirumalai, Structural heterogeneity in transmembrane amyloid precursor protein homodimer is a consequence of environmental selection, J. Am. Chem. Soc. 136 (2014) 9619–9626.
[85] Y. Wang, P.R.L. Markwick, C.A.F. de Oliveira, J.A. McCammon, Enhanced lipid diffusion and mixing in accelerated molecular dynamics, J. Chem. Theory Comput. 7 (2011) 3199–3207.
[86] K. Huang, A.E. Garcia, Acceleration of lateral equilibration in mixed lipid bilayers using replica exchange with solute tempering, J. Chem. Theory Comput. 10 (2014) 4264–4272.
[87] J. Jung, T. Mori, C. Kobayashi, Y. Matsunaga, T. Yoda, M. Feig, Y. Sugita, GENESIS: a hybrid-parallel and multi-scale molecular dynamics simulator with enhanced sampling algorithms for biomolecular and cellular simulations, WIREs Comput. Mol. Sci. 5 (2015) 310–323.
[88] C.J. Cramer, D.G. Truhlar, Implicit solvation models: equilibria, structure, spectra, and dynamics, Chem. Rev. 99 (1999) 2161–2200.
[89] P.A. Kollman, I. Massova, C. Reyes, B. Kuhn, S.H. Huo, L. Chong, M. Lee, T. Lee, Y. Duan, W. Wang, O. Donini, P. Cieplak, J. Srinivasan, D.A. Case, T.E. Cheatham, Calculating structures and free energies of complex molecules: combining molecular mechanics and continuum models, Acc. Chem. Res. 33 (2000) 889–897.
[90] A.W. Gotz, M.J. Williamson, D. Xu, D. Poole, S. Le Grand, R.C. Walker, Routine microsecond molecular dynamics simulations with AMBER on GPUs. 1. Generalized Born, J. Chem. Theory Comput. 8 (2012) 1542–1555.
[91] J.C. Sweet, R.J. Nowling, T. Cickovski, C.R. Sweet, V.S. Pande, J.A. Izaguirre, Long timestep molecular dynamics on the graphical processing unit, J. Chem. Theory Comput. 9 (2013) 3267–3281.
[92] S. Chaudhury, M.A. Olson, G. Tawa, A. Wallqvist, M.S. Lee, Efficient conformational sampling in explicit solvent using a hybrid replica exchange molecular dynamics method, J. Chem. Theory Comput. 8 (2012) 677–687.
[93] R.M. Levy, L.Y. Zhang, E. Gallicchio, A.K. Felts, On the nonpolar hydration free energy of proteins: surface area and continuum solvent models for the solute–solvent interaction energy, J. Am. Chem. Soc. 125 (2003) 9523–9530.
[94] W.C. Still, A. Tempczyk, R.C. Hawley, T. Hendrickson, Semianalytical treatment of solvation for molecular mechanics and dynamics, J. Am. Chem. Soc. 112 (1990) 6127–6129.
[95] D. Sitkoff, K.A. Sharp, B. Honig, Accurate calculation of hydration free-energies using macroscopic solvent models, J. Phys. Chem. 98 (1994) 1978–1988.
[96] J.A. Wagoner, N.A. Baker, Assessing implicit models for nonpolar mean solvation forces: the importance of dispersion and volume terms, Proc. Natl. Acad. Sci. U. S. A. 103 (2006) 8331–8336.
[97] M.E. Davis, J.A. McCammon, Solving the finite-difference linearized Poisson-Boltzmann equation: a comparison of relaxation and conjugate-gradient methods, J. Comput. Chem. 10 (1989) 386–391.
[98] A. Nicholls, B. Honig, A rapid finite-difference algorithm, utilizing successive over-relaxation to solve the Poisson–Boltzmann equation, J. Comput. Chem. 12 (1991) 435–445.
[99] W. Im, D. Beglov, B. Roux, Continuum solvation model: computation of electrostatic forces from numerical solutions to the Poisson–Boltzmann equation, Comput. Phys. Commun. 111 (1998) 59–75.
[100] B. Roux, S. Berneche, W. Im, Ion channels, permeation, and electrostatics: insight into the function of KcsA, Biochemistry 39 (2000) 13295–13306.
[101] I. Oren, S.J. Fleishman, A. Kessel, N. Ben-Tal, Free diffusion of steroid hormones across biomembranes: a simplex search with implicit solvent model calculations, Biophys. J. 87 (2004) 768–779.
[102] B. Roux, Influence of the membrane potential on the free energy of an intrinsic protein, Biophys. J. 73 (1997) 2980–2989.
[103] N.A. Baker, Improving implicit solvent simulations: a Poisson-centric view, Curr. Opin. Struct. Biol. 15 (2005) 137–143.
[104] A. Onufriev, D.A. Case, D. Bashford, Effective Born radii in the generalized Born approximation: the importance of being perfect, J. Comput. Chem. 23 (2002) 1297–1304.
[105] M. Feig, A. Onufriev, M.S. Lee, W. Im, D.A. Case, C.L. Brooks, Performance comparison of generalized Born and Poisson methods in the calculation of electrostatic solvation energies for protein structures, J. Comput. Chem. 25 (2004) 265–284.
[106] G.D. Hawkins, C.J. Cramer, D.G. Truhlar, Parametrized models of aqueous free energies of solvation based on pairwise descreening of solute atomic charges from a dielectric medium, J. Phys. Chem. 100 (1996) 19824–19839.
[107] D. Qiu, P.S. Shenkin, F.P. Hollinger, W.C. Still, The GB/SA continuum model for solvation. A fast analytical method for the calculation of approximate Born radii, J. Phys. Chem. A 101 (1997) 3005–3014.
[108] B.N. Dominy, C.L. Brooks, Development of a generalized Born model parametrization for proteins and nucleic acids, J. Phys. Chem. B 103 (1999) 3765–3773.
[109] M. Scarsi, J. Apostolakis, A. Caflisch, Continuum electrostatic energies of macromolecules in aqueous solutions, J. Phys. Chem. A 101 (1997) 8098–8106.
[110] A. Ghosh, C.S. Rapp, R.A. Friesner, Generalized Born model based on a surface integral formulation, J. Phys. Chem. B 102 (1998) 10983–10990.
[111] M.S. Lee, F.R. Salsbury, C.L. Brooks, Novel generalized Born methods, J. Chem. Phys. 116 (2002) 10606–10614.
[112] M.S. Lee, M. Feig, F.R. Salsbury, C.L. Brooks, New analytic approximation to the standard molecular volume definition and its application to generalized Born calculations, J. Comput. Chem. 24 (2003) 1348–1356.
[113] J. Mongan, C. Simmerling, J.A. McCammon, D.A. Case, A. Onufriev, Generalized Born model with a simple, robust molecular volume correction, J. Chem. Theory Comput. 3 (2007) 156–169.
[114] A. Onufriev, D. Bashford, D.A. Case, Exploring protein native states and large-scale conformational changes with a modified generalized Born model, Proteins 55 (2004) 383–394.
[115] W.P. Im, M.S. Lee, C.L. Brooks, Generalized Born model with a simple smoothing function, J. Comput. Chem. 24 (2003) 1691–1702.
[116] H.A. Stern, S.E. Feller, Calculation of the dielectric permittivity profile for a nonuniform system: application to a lipid bilayer simulation, J. Chem. Phys. 118 (2003) 3401–3412.
[117] H. Nymeyer, H.X. Zhou, A method to determine dielectric constants in nonhomogeneous systems: application to biological membranes, Biophys. J. 94 (2008) 1185–1193.
[118] V.Z. Spassov, L. Yan, S. Szalma, Introducing an implicit membrane in generalized Born/solvent accessibility continuum solvent models, J. Phys. Chem. B 106 (2002) 8726–8738.
[119] W. Im, M. Feig, C.L. Brooks, An implicit membrane generalized Born theory for the study of structure, stability, and interactions of membrane proteins, Biophys. J. 85 (2003) 2900–2918.
[120] S. Tanizaki, M. Feig, A generalized Born formalism for heterogeneous dielectric environments: application to the implicit modeling of biological membranes, J. Chem. Phys. 122 (2005) 124706.
[121] S.J. Marrink, H.J.C. Berendsen, Permeation process of small molecules across lipid membranes studied by molecular dynamics simulations, J. Phys. Chem. 100 (1996) 16729–16738.
[122] A. Panahi, M. Feig, Dynamic heterogeneous dielectric generalized Born (DHDGB): an implicit membrane model with a dynamically varying bilayer thickness, J. Chem. Theory Comput. 9 (2013) 1709–1719.
[123] T. Lazaridis, Effective energy function for proteins in lipid membranes, Proteins 52 (2003) 176–192.
[124] T. Lazaridis, M. Karplus, Effective energy function for proteins in solution, Proteins 35 (1999) 133–152.
[125] O. Yuzlenko, T. Lazaridis, Membrane protein native state discrimination by implicit membrane models, J. Comput. Chem. 34 (2013) 731–738.
[126] M. Mottamal, T. Lazaridis, Voltage-dependent energetics of alamethicin monomers in the membrane, Biophys. Chem. 122 (2006) 50–57.
[127] H. Zhan, T. Lazaridis, Influence of the membrane dipole potential on peptide binding to lipid bilayers, Biophys. Chem. 161 (2012) 1–7.

[128] T. Lazaridis, Structural determinants of transmembrane β-barrels, J. Chem. Theory Comput. 1 (2005) 716–722.
[129] M. Mihajlovic, T. Lazaridis, Antimicrobial peptides bind more strongly to membrane pores, Biochim. Biophys. Acta Biomembr. 1798 (2010) 1494–1502.
[130] T. Lazaridis, Implicit solvent simulations of peptide interactions with anionic lipid membranes, Proteins 58 (2005) 518–527.
[131] H. Zhan, T. Lazaridis, Inclusion of lateral pressure/curvature stress effects in implicit membrane models, Biophys. J. 104 (2013) 643–654.
[132] R.S. Cantor, Lipid composition and the lateral pressure profile in bilayers, Biophys. J. 76 (1999) 2625–2639.
[133] B.R. Brooks, C.L. Brooks, A.D. Mackerell, L. Nilsson, R.J. Petrella, B. Roux, Y. Won, G. Archontis, C. Bartels, S. Boresch, A. Caflisch, L. Caves, Q. Cui, A.R. Dinner, M. Feig, S. Fischer, J. Gao, M. Hodoscek, W. Im, K. Kuczera, T. Lazaridis, J. Ma, V. Ovchinnikov, E. Paci, R.W. Pastor, C.B. Post, J.Z. Pu, M. Schaefer, B. Tidor, R.M. Venable, H.L. Woodcock, X. Wu, W. Yang, D.M. York, M. Karplus, CHARMM: the biomolecular simulation program, J. Comput. Chem. 30 (2009) 1545–1614.
[134] R. Salomon-Ferrer, D.A. Case, R.C. Walker, An overview of the Amber biomolecular simulation package, WIREs Comput. Mol. Sci. 3 (2013) 198–210.
[135] J.C. Phillips, R. Braun, W. Wang, J. Gumbart, E. Tajkhorshid, E. Villa, C. Chipot, R.D. Skeel, L. Kale, K. Schulten, Scalable molecular dynamics with NAMD, J. Comput. Chem. 26 (2005) 1781–1802.
[136] S. Pronk, S. Pall, R. Schulz, P. Larsson, P. Bjelkmar, R. Apostolov, M.R. Shirts, J.C. Smith, P.M. Kasson, D. van der Spoel, B. Hess, E. Lindahl, GROMACS 4.5: a high-throughput and highly parallel open source molecular simulation toolkit, Bioinformatics 29 (2013) 845–854.
[137] J.W. Ponder, TINKER: Software Tools for Molecular Fesign, 7.1 ed. Washington University School of Medicine, Saint Louis, MO, 2015.
[138] J.L. Banks, H.S. Beard, Y.X. Cao, A.E. Cho, W. Damm, R. Farid, A.K. Felts, T.A. Halgren, D.T. Mainz, J.R. Maple, R. Murphy, D.M. Philipp, M.P. Repasky, L.Y. Zhang, B.J. Berne, R.A. Friesner, E. Gallicchio, R.M. Levy, Integrated modeling program, applied chemical theory (IMPACT), J. Comput. Chem. 26 (2005) 1752–1780.
[139] S. Jo, M. Vargyas, J. Vasko-Szedlar, B. Roux, W. Im, PBEQ-solver for online visualization of electrostatic potential of biomolecules, Nucleic Acids Res. 36 (2008) W270–W275.
[140] M.S. Friedrichs, P. Eastman, V. Vaidyanathan, M. Houston, S. Legrand, A.L. Beberg, D.L. Ensign, C.M. Bruns, V.S. Pande, Accelerating molecular dynamic simulation on graphics processing units, J. Comput. Chem. 30 (2009) 864–872.
[141] C. Kutzner, S. Pall, M. Fechner, A. Esztermann, B.L. de Groot, H. Grubmuller, Best bang for your buck: GPU nodes for GROMACS biomolecular simulations, J. Comput. Chem. 36 (2015) 1990–2008.
[142] D.E. Tanner, J.C. Phillips, K. Schulten, GPU/CPU algorithm for generalized Born/solvent-accessible surface area implicit solvent calculations, J. Chem. Theory Comput. 8 (2012) 2521–2530.
[143] U. Essmann, L. Perera, M.L. Berkowitz, T. Darden, H. Lee, L.G. Pedersen, A smooth particle mesh Ewald method, J. Chem. Phys. 103 (1995) 8577–8593.
[144] J. Jung, C. Kobayashi, T. Imamura, Y. Sugita, Parallel implementation of 3D FFT with volumetric decomposition schemes for efficient molecular dynamics simulations, Comput. Phys. Commun., http://dx.doi.org/10.1016/j.cpc.2015.10.024.
[145] R. Anandakrishnan, M. Daga, A.V. Onufriev, An n log n generalized Born approximation, J. Chem. Theory Comput. 7 (2011) 544–559.
[146] D.E. Tanner, K.Y. Chan, J.C. Phillips, K. Schulten, Parallel generalized Born implicit solvent calculations with NAMD, J. Chem. Theory Comput. 7 (2011) 3635–3642.
[147] G. Lamoureux, A.D. MacKerell, B. Roux, A simple polarizable model of water based on classical Drude oscillators, J. Chem. Phys. 119 (2003) 5185–5197.
[148] J. Chowdhary, E. Harder, P.E.M. Lopes, L. Huang, A.D. MacKerell, B. Roux, A polarizable force field of dipalmitoylphosphatidylcholine based on the classical drude model for molecular dynamics simulations of lipids, J. Phys. Chem. B 117 (2013) 9142–9160.
[149] M. Patra, M. Karttunen, M.T. Hyvonen, E. Falck, P. Lindqvist, I. Vattulainen, Molecular dynamics simulations of lipid bilayers: major artifacts due to truncating electrostatic interactions, Biophys. J. 84 (2003) 3636–3645.
[150] A.D. MacKerell Jr., D. Bashford, M. Bellott, R.L. Dunbrack Jr., J.D. Evanseck, M.J. Field, S. Fischer, J. Gao, H. Guo, S. Ha, D. Joseph-McCarthy, L. Kuchnir, K. Kuczera, F.T.K. Lau, C. Mattos, S. Michnick, T. Ngo, D.T. Nguyen, B. Prodhom, W.E. Reiher III, B. Roux, M. Schlenkrich, J.C. Smith, R. Stote, J. Straub, M. Watanabe, J. Wiórkiewicz-Kuczera, D. Yin, M. Karplus, All-atom empirical potential for molecular modeling and dynamics studies of proteins, J. Phys. Chem. B 102 (1998) 3586–3616.
[151] A.A. Skjevik, B.D. Madej, R.C. Walker, K. Teigen, LIPID11: a modular framework for lipid simulations using amber, J. Phys. Chem. B 116 (2012) 11124–11136.
[152] R.W. Pastor, A.D. MacKerell, Development of the CHARMM force field for lipids, J. Phys. Chem. Lett. 2 (2011) 1526–1532.
[153] Y. Zhang, S.E. Feller, B.R. Brooks, R.W. Pastor, Computer simulation of liquid/liquid interfaces. I. Theory and application to octane/water, J. Chem. Phys. 103 (1995) 10252–10266.
[154] M.A. Lomize, A.L. Lomize, I.D. Pogozheva, H.I. Mosberg, OPM: orientations of proteins in membranes database, Bioinformatics 22 (2006) 623–625.
[155] S. Jo, T. Kim, W. Im, Automated builder and database of protein/membrane complexes for molecular dynamics simulations, PLoS One 2 (2007), e880.
[156] C. Kandt, W.L. Ash, D.P. Tieleman, Setting up and running molecular dynamics simulations of membrane proteins, Methods 41 (2007) 475–488.
[157] M. Javanainen, Universal method for embedding proteins into complex lipid bilayers for molecular dynamics simulations, J. Chem. Theory Comput. 10 (2014) 2577–2582.
[158] M.M. Ghahremanpour, S.S. Arab, S.B. Aghazadeh, J. Zhang, D. van der Spoel, MemBuilder: a web-based graphical interface to build heterogeneously mixed membrane bilayers for the GROMACS biomolecular simulation program, Bioinformatics 30 (2014) 439–441.
[159] P.J. Stansfeld, J.E. Goose, M. Caffrey, E.P. Carpenter, J.L. Parker, S. Newstead, M.S.P. Sansom, MemProtMD: automated insertion of membrane protein structures into explicit lipid membranes, Structure 23 (2015) 1350–1361.
[160] S. Jo, J.B. Lim, J.B. Klauda, W. Im, CHARMM-GUI membrane builder for mixed bilayers and its application to yeast membranes, Biophys. J. 97 (2009) 50–58.
[161] E.L. Wu, X. Cheng, S. Jo, H. Rui, K.C. Song, E.M. Davila-Contreras, Y.F. Qi, J.M. Lee, V. Monje-Galvan, R.M. Venable, J.B. Klauda, W. Im, CHARMM-GUI membrane builder toward realistic biological membrane simulations, J. Comput. Chem. 35 (2014) 1997–2004.
[162] J. Lee, X. Cheng, J.M. Swails, M.S. Yeom, P.K. Estman, J.A. Lemkul, S. Wei, J. Buckner, J.C. Jeong, Y. Qi, S. Jo, V.S. Pande, D.A. Case, C.L. Brooks, A.D. MacKerell, J.B. Klauda, W. Im, CHARMM-GUI Input Generator for NAMD, GROMACS, AMBER, OpenMM, and CHARMM/OpenMM simulations using the CHARMM36 additive force field, J. Chem. Theory Comput., http://dx.doi.org/10.1021/acs.jctc.5b00935.
[163] S. Park, A.H. Beayen, J.B. Klauda, W. Im, How tolerant are membrane simulations with mismatch in area per lipid between leaflets? J. Chem. Theory Comput. 11 (2015) 3466–3477.
[164] T. Mori, F. Ogushi, Y. Sugita, Analysis of lipid surface area in protein–membrane systems combining Voronoi tessellation and Monte Carlo integration methods, J. Comput. Chem. 33 (2011) 286–293.
[165] S. Takada, Coarse-grained molecular simulations of large biomolecules, Curr. Opin. Struct. Biol. 22 (2012) 130–137.
[166] D. Hakobyan, A. Heuer, Phase separation in a lipid/cholesterol system: comparison of coarse-grained and united-atom simulations, J. Phys. Chem. B 117 (2013) 3841–3851.
[167] J.E. Goose, M.S.P. Sansom, Reduced lateral mobility of lipids and proteins in crowded membranes, PLoS Comput. Biol. 9 (2013), e1003033.
[168] K.P. Santo, M.L. Berkowitz, Difference between magainin-2 and melittin assemblies in phosphatidylcholine bilayers: results from coarse-grained simulations, J. Phys. Chem. B 116 (2012) 3021–3030.
[169] M. Louhivuori, H.J. Risselada, E. van der Giessen, S.J. Marrink, Release of content through mechano-sensitive gates in pressurized liposomes, Proc. Natl. Acad. Sci. U. S. A. 107 (2010) 19856–19860.
[170] M. Seo, S. Rauscher, R. Pomes, D.P. Tieleman, Improving internal peptide dynamics in the coarse-grained MARTINI model: toward large-scale simulations of amyloid- and elastin-like peptides, J. Chem. Theory Comput. 8 (2012) 1774–1785.
[171] G.S. Ayton, G.A. Voth, Systematic multiscale simulation of membrane protein systems, Curr. Opin. Struct. Biol. 19 (2009) 138–144.
[172] S.M. Gopal, S. Mukherjee, Y.M. Cheng, M. Feig, PRIMO/PRIMONA: a coarse-grained model for proteins and nucleic acids that preserves near-atomistic accuracy, Proteins 78 (2010) 1266–1281.
[173] P. Kar, S.M. Gopal, Y.M. Cheng, A. Predeus, M. Feig, PRIMO: a transferable coarse-grained force field for proteins, J. Chem. Theory Comput. 9 (2013) 3769–3788.
[174] W. Han, Y.D. Wu, Coarse-grained protein model coupled with a coarse-grained water model: molecular dynamics study of polyalanine-based peptides, J. Chem. Theory Comput. 3 (2007) 2146–2161.
[175] Y.F. Qi, X. Cheng, W. Han, S. Jo, K. Schulten, W. Im, CHARMM-GUI PACE CG builder for solution, micelle, and bilayer coarse-grained simulations, J. Chem. Inf. Model. 54 (2014) 1003–1009.
[176] Y.F. Qi, H.I. Ingolfsson, X. Cheng, J. Lee, S.J. Marrink, W. Im, CHARMM-GUI martini maker for coarse-grained simulations with the martini force field, J. Chem. Theory Comput. 11 (2015) 4486–4494.
[177] T. Okabe, M. Kawata, Y. Okamoto, M. Mikami, Replica-exchange Monte Carlo method for the isobaric–isothermal ensemble, Chem. Phys. Lett. 335 (2001) 435–439.
[178] G.J. Martyna, D.J. Tobias, M.L. Klein, Constant pressure molecular dynamics algorithms, J. Chem. Phys. 101 (1994) 4177–4189.
[179] Y. Mori, Y. Okamoto, Generalized-ensemble algorithms for the isobaric–isothermal ensemble, J. Phys. Soc. Jpn. 79 (2010) 074003.
[180] Y. Mori, Y. Okamoto, Replica-exchange molecular dynamics simulations for various constant temperature algorithms, J. Phys. Soc. Jpn. 79 (2010) 074001.
[181] A.M. Ferrenberg, R.H. Swendsen, New Monte-Carlo technique for studying phase-transitions, Phys. Rev. Lett. 61 (1988) 2635–2638.
[182] S. Kumar, D. Bouzida, R.H. Swendsen, P.A. Kollman, J.M. Rosenberg, The weighted histogram analysis method for free-energy calculations on biomolecules. I. The method, J. Comput. Chem. 13 (1992) 1011–1021.
[183] G.M. Torrie, J.P. Valleau, Non-physical sampling distributions in Monte-Carlo free-energy estimation: umbrella sampling, J. Comput. Phys. 23 (1977) 187–199.
[184] E.M. Boczko, C.L. Brooks, Constant-temperature free-energy surfaces for physical and chemical processes, J. Phys. Chem. 97 (1993) 4509–4513.
[185] J.L. Knight, C.L. Brooks, λ-Dynamics free energy simulation methods, J. Comput. Chem. 30 (2009) 1692–1700.
[186] H. Fukunishi, O. Watanabe, S. Takada, On the Hamiltonian replica exchange method for efficient sampling of biomolecular systems: application to protein structure prediction, J. Chem. Phys. 116 (2002) 9058–9067.
[187] S. Park, T. Kim, W. Im, Transmembrane helix assembly by window exchange umbrella sampling, Phys. Rev. Lett. 108 (2012) 108102.
[188] F. Jähnig, What is the surface tension of a lipid bilayer membrane? Biophys. J. 71 (1996) 1348–1349.
[189] H.J. Galla, W. Hartmann, U. Theilen, E. Sackmann, 2-Dimensional passive random-walk in lipid bilayers and fluid pathways in biomembranes, J. Membr. Biol. 48 (1979) 215–236.
[190] T. Terakawa, T. Kameda, S. Takada, On easy implementation of a variant of the replica exchange with solute tempering in GROMACS, J. Comput. Chem. 32 (2011) 1228–1234.

[191] L.L. Wang, R.A. Friesner, B.J. Berne, Replica exchange with solute scaling: a more efficient version of replica exchange with solute tempering (REST2), J. Phys. Chem. B 115 (2011) 9431–9438.
[192] S.L.C. Moors, S. Michielssens, A. Ceulemans, Improved replica exchange method for native-state protein sampling, J. Chem. Theory Comput. 7 (2011) 231–237.
[193] Y.L. Miao, V.A. Feher, J.A. McCammon, Gaussian accelerated molecular dynamics: unconstrained enhanced sampling and free energy calculation, J. Chem. Theory Comput. 11 (2015) 3584–3595.
[194] K.R. MacKenzie, J.H. Prestegard, D.M. Engelman, A transmembrane helix dimer: structure and implications, Science 276 (1997) 131–133.
[195] K.S. Mineev, E.V. Bocharov, P.E. Volynsky, M.V. Goncharuk, E.N. Tkach, Y.S. Ermolyuk, A.A. Schulga, V.V. Chupin, I.V. Maslennikov, R.G. Efremov, A.S. Arseniev, Dimeric structure of the transmembrane domain of glycophorin A in lipidic and detergent environments, Acta Nat. 3 (2011) 90–98.
[196] S.O. Smith, D. Song, S. Shekar, M. Groesbeek, M. Ziliox, S. Aimoto, Structure of the transmembrane dimer interface of glycophorin A in membrane bilayers, Biochemistry 40 (2001) 6553–6558.
[197] H. Hong, J.U. Bowie, Dramatic destabilization of transmembrane helix interactions by features of natural membrane environments, J. Am. Chem. Soc. 133 (2011) 11389–11398.
[198] H. Kokubo, Y. Okamoto, Prediction of membrane protein structures by replica-exchange Monte Carlo simulations: case of two helices, J. Chem. Phys. 120 (2004) 10837–10847.
[199] W.P. Russ, D.M. Engelman, The GxxxG motif: a framework for transmembrane helix–helix association, J. Mol. Biol. 296 (2000) 911–919.
[200] A. Senes, M. Gerstein, D.M. Engelman, Statistical analysis of amino acid patterns in transmembrane helices: the GxxxG motif occurs frequently and in association with β-branched residues at neighboring positions, J. Mol. Biol. 296 (2000) 921–936.
[201] J.L. Popot, D.M. Engelman, Membrane–protein folding and oligomerization: the two-stage model, Biochemistry 29 (1990) 4031–4037.
[202] J. Lee, W. Im, Implementation and application of helix–helix distance and crossing angle restraint potentials, J. Comput. Chem. 28 (2007) 669–680.
[203] J. Lee, W. Im, Role of hydrogen bonding and helix–lipid interactions in transmembrane helix association, J. Am. Chem. Soc. 130 (2008) 6456–6462.
[204] D.H. MacLennan, E.G. Kranias, Phospholamban: a crucial regulator of cardiac contractility, Nat. Rev. Mol. Cell Biol. 4 (2003) 566–577.
[205] J. Zamoon, A. Mascioni, D.D. Thomas, G. Veglia, NMR solution structure and topological orientation of monomeric phospholamban in dodecylphosphocholine micelles, Biophys. J. 85 (2003) 2589–2598.
[206] L.G. Reddy, L.R. Jones, D.D. Thomas, Depolymerization of phospholamban in the presence of calcium pump: a fluorescence energy transfer study, Biochemistry 38 (1999) 3954–3962.
[207] R.L. Cornea, L.R. Jones, J.M. Autry, D.D. Thomas, Mutation and phosphorylation change the oligomeric structure of phospholamban in lipid bilayers, Biochemistry 36 (1997) 2960–2967.
[208] N.J. Traaseth, L. Shi, R. Verardi, D.G. Mullen, G. Barany, G. Veglia, Structure and topology of monomeric phospholamban in lipid membranes determined by a hybrid solution and solid-state NMR approach, Proc. Natl. Acad. Sci. U. S. A. 106 (2009) 10165–10170.
[209] K. Oxenoid, J.J. Chou, The structure of phospholamban pentamer reveals a channel-like architecture in membranes, Proc. Natl. Acad. Sci. U. S. A. 102 (2005) 10870–10875.
[210] R. Verardi, L. Shi, N.J. Traaseth, N. Walsh, G. Veglia, Structural topology of phospholamban pentamer in lipid bilayers by a hybrid solution and solid-state NMR method, Proc. Natl. Acad. Sci. U. S. A. 108 (2011) 9101–9106.
[211] M. Tada, M.A. Kirchberger, A.M. Katz, Regulation of calcium transport in cardiac sarcoplasmic reticulum by cyclic AMP-dependent protein kinase, Recent Adv. Stud. Cardiac Struct. Metab. 9 (1976) 225–239.
[212] M. Tada, M. Inui, M. Yamada, M. Kadoma, T. Kuzuya, H. Abe, S. Kakiuchi, Effects of phospholamban phosphorylation catalyzed by adenosine 3′:5′-monophosphate- and calmodulin-dependent protein kinases on calcium transport ATPase of cardiac sarcoplasmic reticulum, J. Mol. Cell. Cardiol. 15 (1983) 335–346.
[213] P. James, M. Inui, M. Tada, M. Chiesi, E. Carafoli, Nature and site of phospholamban regulation of the Ca^{2+} pump of sarcoplasmic reticulum, Nature 342 (1989) 90–92.
[214] C. Toyoshima, M. Asahi, Y. Sugita, R. Khanna, T. Tsuda, D.H. MacLennan, Modeling of the inhibitory interaction of phospholamban with the Ca^{2+} ATPase, Proc. Natl. Acad. Sci. U. S. A. 100 (2003) 467–472.
[215] B.L. Akin, T.D. Hurley, Z. Chen, L.R. Jones, The structural basis for phospholamban inhibition of the calcium pump in sarcoplasmic reticulum, J. Biol. Chem. 288 (2013) 30181–30191.
[216] E.E. Metcalfe, N.J. Traaseth, G. Veglia, Serine 16 phosphorylation induces an order-to-disorder transition in monomeric phospholamban, Biochemistry 44 (2005) 4386–4396.
[217] C. Haass, D.J. Selkoe, Soluble protein oligomers in neurodegeneration: lessons from the Alzheimer's amyloid β-peptide, Nat. Rev. Mol. Cell Biol. 8 (2007) 101–112.
[218] J. Kang, H.G. Lemaire, A. Unterbeck, J.M. Salbaum, C.L. Masters, K.H. Grzeschik, G. Multhaup, K. Beyreuther, B. Mullerhill, The precursor of Alzheimer's disease amyloid A4 protein resembles a cell-surface receptor, Nature 325 (1987) 733–736.
[219] R. Vassar, M. Citron, Aβ-generating enzymes: recent advances in β- and γ-secretase research, Neuron 27 (2000) 419–422.
[220] J.E. Straub, D. Thirumalai, Toward a molecular theory of early and late events in monomer to amyloid fibril formation, Annu. Rev. Phys. Chem. 62 (2011) 437–463.
[221] A.J. Beel, C.K. Mobley, H.J. Kim, F. Tian, A. Hadziselimovic, B. Jap, J.H. Prestegard, C.R. Sanders, Structural studies of the transmembrane C-terminal domain of the amyloid precursor protein (APP): does APP function as a cholesterol sensor? Biochemistry 47 (2008) 9428–9446.
[222] P.J. Barrett, Y.L. Song, W.D. Van Horn, E.J. Hustedt, J.M. Schafer, A. Hadziselimovic, A.J. Beel, C.R. Sanders, The amyloid precursor protein has a flexible transmembrane domain and binds cholesterol, Science 336 (2012) 1168–1171.
[223] L.M. Munter, P. Voigt, A. Harmeier, D. Kaden, K.E. Gottschalk, C. Weise, R. Pipkorn, M. Schaefer, D. Langosch, G. Multhaup, GxxxG motifs within the amyloid precursor protein transmembrane sequence are critical for the etiology of Aβ42, EMBO J. 26 (2007) 1702–1712.
[224] P. Kienlen-Campard, B. Tasiaux, J. Van Hees, M. Li, S. Huysseune, T. Sato, J.Z. Fei, S. Aimoto, P.J. Courtoy, S.O. Smith, S.N. Constantinescu, J.N. Octave, Amyloidogenic processing but not amyloid precursor protein (APP) intracellular C-terminal domain production requires a precisely oriented APP dimer assembled by transmembrane GXXXG motifs, J. Biol. Chem. 283 (2008) 7733–7744.
[225] K.D. Nadezhdin, O.V. Bocharova, E.V. Bocharov, A.S. Arseniev, Dimeric structure of transmembrane domain of amyloid precursor protein in micellar environment, FEBS Lett. 586 (2012) 1687–1692.
[226] C. Hong, D.P. Tieleman, Y. Wang, Microsecond molecular dynamics simulations of lipid mixing, Langmuir 30 (2014) 11993–12001.
[227] W.N. E, E. Vanden-Eijnden, Transition-path theory and path-finding algorithms for the study of rare events, Annu. Rev. Phys. Chem. 61 (2010) 391–420.
[228] M. Moradi, E. Tajkhorshid, Computational recipe for efficient description of large-scale conformational changes in biomolecular systems, J. Chem. Theory Comput. 10 (2014) 2866–2880.
[229] M. Moradi, E. Tajkhorshid, Mechanistic picture for conformational transition of a membrane transporter at atomic resolution, Proc. Natl. Acad. Sci. U. S. A. 110 (2013) 18916–18921.
[230] M. Moradi, G. Enkavi, E. Tajkhorshid, Atomic-level characterization of transport cycle thermodynamics in the glycerol-3-phosphate:phosphate antiporter, Nat. Commun. 6 (2015) 8393.
[231] C.R. Schwantes, R.T. McGibbon, V.S. Pande, Perspective: Markov models for long-timescale biomolecular dynamics, J. Chem. Phys. 141 (2014) 090901.
[232] J.D. Chodera, F. Noe, Markov state models of biomolecular conformational dynamics, Curr. Opin. Struct. Biol. 25 (2014) 135–144.
[233] K.J. Kohlhoff, D. Shukla, M. Lawrenz, G.R. Bowman, D.E. Konerding, D. Belov, R.B. Altman, V.S. Pande, Cloud-based simulations on Google exacycle reveal ligand modulation of GPCR activation pathways, Nat. Chem. 6 (2014) 15–21.
[234] Y.L. Miao, S.E. Nichols, J.A. McCammon, Free energy landscape of G-protein coupled receptors, explored by accelerated molecular dynamics, Phys. Chem. Chem. Phys. 16 (2014) 6398–6406.
[235] R. Singh, N. Ahalawat, R.K. Murarka, Activation of corticotropin-releasing factor 1 receptor: insights from molecular dynamics simulations, J. Phys. Chem. B 119 (2015) 2806–2817.